Structural Engineering and Mechanics, *Vol. 64, No. 5 (2017) 591-610*
DOI: https://doi.org/10.12989/sem.2017.64.5.591

Static analysis of non-uniform heterogeneous circular plate with porous material resting on a gradient hybrid foundation involving friction force

A. Behravan Rad[*1], M.R. Farzan-Rad[2a] and K. Mohammadi Majd[1b]

[1]*Engineering Department, Zamyad Company, 15 Km Karaj Old Road, P.O 1386183741, Tehran, Iran*
[2]*Ministry of Education, Shahryar Branch, 3351739155, Shahryar, Iran*

(Received February 19, 2017, Revised August 15, 2017, Accepted August 18, 2017)

Abstract. This paper is concerned with the static analysis of variable thickness of two directional functionally graded porous materials (FGPM) circular plate resting on a gradient hybrid foundation (Horvath-Colasanti type) with friction force and subjected to compound mechanical loads (e.g., transverse, in-plane shear traction and concentrated force at the center of the plate).The governing state equations are derived in terms of displacements based on the 3D theory of elasticity, assuming the elastic coefficients of the plate material except the Poisson's ratio varying continuously throughout the thickness and radial directions according to an exponential function. These equations are solved semi-analytically by employing the state space method (SSM) and one-dimensional differential quadrature (DQ) rule to obtain the displacements and stress components of the FGPM plate. The effect of concentrated force at the center of the plate is approximated with the shear force, uniformly distributed over the inner boundary of a FGPM annular plate. In addition to verification study and convergence analysis, numerical results are displayed to show the effect of material heterogeneity indices, foundation stiffness coefficients, foundation gradient indices, loads ratio, thickness to radius ratio, compressibility, porosity and friction coefficient of the foundation on the static behavior of the plate. Finally, the responses of FG and FG porous material circular plates to compound mechanical loads are compared.

Keywords: functionally graded Porous material; heterogeneous hybrid foundation; circular plate; elasticity; compressibility; porosity; semi-analytical method; friction

1. Introduction

In recent years, new class of advanced composite materials known as functionally graded porous materials (FGPM) has introduced in the literature and attracted a lot of attention by researchers. These materials have found practical applications in many scientific and engineering fields (i.e., aerospace, vehicles, civil, mechanical, nuclear and biomedical) due to their smooth variation in properties. On the other hand, the modeling, analysis and optimization of basic structures (beams, plates and shells) interacting with the elastic foundations is a topic in engineering. As basic structural elements, circular plates composed from heterogeneous porous materials supported by elastic foundations have found a wide range of engineering applications. Typical examples may be found in the design and analysis of interaction between structure and foundation of storage tanks and silos, driven plates of friction clutches and brake disks of machine tools and vehicles. Besides, in modern engineering this topic may be used to formulate the effect of the artificial organs interacting with the biological medium and nano-plates embedded in an elastomeric substrate.

Taking into account the plate theories, many researchers have been used analytical methods to study the static bending, buckling behavior, vibration problems and dynamic response of heterogeneous circular plates. In this regard, axisymmetric bending of thick functionally graded circular plates with various outer edge conditions was studied by Saidi *et al*. (2009), based on third order shear deformation plate theory. Fallah and coauthors (2012, 2015) used first-order shear deformation plate theory (FSDT) with Von Karman geometric non-linearity to investigate the bending and post-buckling behaviors of FG circular plates under asymmetric loading in conjunction with thermal loading and in-plane loading. On the basis of the classical plate theory (CPT), Khorshidvand *et al*. (2014) obtained the critical buckling load of porous circular plate integrated with piezoelectric sensor-actuator layers under uniform radial compression. They employed the energy method and calculus of variations to derive the governing equations and carried out an eigenvalue solution for the plate with clamped edge. Utilizing CPT and FSDT theories, Jabbari *et al*. (2014a, b, c) studied the buckling of a porous circular plate. They investigated the effect of porosity and pore fluid properties on the critical buckling load. They also studied the effect of thermal load and constant applied voltage on piezoelectric layers. In other investigation, Jabbari *et al*. (2013) developed an analytical method to obtain the steady

∗Corresponding author, Ph.D.
E-mail: behravanrad@gmail.com, abehravanrad@aol.com
[a]Msc
E-mail: farzanreza@gmail.com
[b]Msc
E-mail: kamalmajd@gmail.com

ISSN: 1225-4568 (Print), 1598-6217 (Online)

state thermal and mechanical stresses of a poro-piezo-FGM hollow sphere. Farzaneh Joubaneh *et al*. (2015) provided an analysis to obtain the critical buckling temperature of porous circular plates integrated with piezoelectric sensor-actuator patches under uniform thermal load. They obtained the governing equations, based on the CPT**,** by employing the energy method and calculus of variations. They also assumed the material properties of porous plate to vary by a power law distribution through the thickness of the plate, and the plate pores are saturated with fluid. Mojahedin *et al*. (2016) used the higher order shear deformation plate theory (HSDT) to obtain the pre-buckling force and critical buckling loads of porous FGM circular plates. They derived the equilibrium and stability equations by using energy method and the calculus of variations, and considering the Sanders non-linear strain-displacement relations. Chen *et al*. (2015) used the Timoshenko beam theory to accomplish the static bending and buckling analysis of functionally graded porous beams. Benferhat *et al*. (2016) used sinusoidal shear deformation theory and presented an analytical solution to investigate the effect of porosity on bending and free vibration behavior of simply supported FG rectangular plate resting on Winkler-Pasternak foundation. Recently, Akbas (2017) employed finite element and Newton-Raphson methods to analyze the post-buckling of FG beams with porosity effect under compression load. Using the Runge-Kutta method and deformation map approach, the axially symmetric deformations and stability of a geometrically nonlinear circular plate subjected to multiparametrical static loading have been investigated by Drawshi and Betten (1992).

Differential quadrature (DQ) method as an efficient and accurate numerical tool has been used to study the bending, buckling, thermoelastic and dynamic behavior of homogeneous and heterogeneous circular plates under various loads. Civalek and Ulker (2004) used the harmonic differential quadrature (HDQ) method to predict the linear bending behavior of circular plates. In other study, Civalek (2004a) applied the DQ and HDQ methods to illustrate the bending, buckling and free vibration analysis of thin isotropic plates and elastic columns. Considering the 2D thermo-elasticity theory, Sepahi *et al*. (2010) used the DQ method for axisymmetric large deflection response of a simply supported annular FG plate resting on a nonlinear elastic foundation (Pasternak type). Taking into account the first order shear deformation theory (FSDT) and adopting this technique, Malekzadeh *et al*. (2011) studied the free vibration of temperature-dependent functionally graded annular plates on elastic foundations. The free vibration problem of the thick FG annular plates on an elastic foundation was investigated by the Yas and Tahouneh (2012) based on the 3D theory of elasticity. On the basis of the classical plate theory (CPT), Kumar and Lal (2013) predicted the free axisymmetric vibration of two directional functionally graded annular plates resting on a Winkler foundation**,** using DQ method and Chebyshev collocation technique. In their study power law type property distribution in both thickness and radial directions is considered. Baccicchi and coauthors (2015, 2016) studied the vibration characteristic of variable thickness plates, shells and doubly-curved shells using GDQ method.

The differential transformation method (DTM)**,** based on the Taylor series expansion**,** is one of the mathematical techniques which has been used to solve the differential equation of structures in recent years. Shariyat and Alipour (2011) considered the classical plate theory and DTM to analyze the free vibration and modal stress of two-directional functionally graded circular plates embedded on two-parameter elastic foundations. The static behavior of FG circular plates with power law distribution of constituents resting on a Winkler-type elastic foundation was studied by Abbasi *et al*. (2014). On the basis of the Mindilin's shear deformation plate theory and assuming the material properties of the FG circular plate to vary in the transverse direction by a power-law and exponentially in the radial direction, Alipour and Shariyat (2013) analyzed the buckling behavior of variable thickness of 2D-FGM circular plates resting on non-uniform elastic foundations by using DTM. Lal and Ahlawat (2015a, b) employed the CPT and DTM to analyze the buckling and vibration behaviors of uniform and non-uniform FG circular plates resting on Winkler foundation.

Numerous investigations have been analytically reported in the literature to characterize the bending, dynamic and thermoelastic behavior of FG and smart functionally graded porous material structures. Li *et al*. (2008) obtained elasticity solutions for transversely isotropic FG circular plates subjected to an axisymmetric transverse load in the form of an even order polynomials (e.g., $q\, r^k$, k is zero or a finite even integer). On the basis of the three dimensional theory and utilizing direct displacement method, Wang *et al*. (2010, 2016) presented an analytical solution for the axisymmetric bending of FG circular plate and the FG annular plates made of magneto-electro-elastic and piezoelectric materials, respectively. Sburlati and Bardella (2011) developed a three-dimensional elasticity solution for the bending problem of the FG thick circular plates subjected to axisymmetric conditions. The equilibrium equations are described in terms of the potential functions based on Plevako's representation. The material properties were varied along the thickness of the plate. Assuming the material properties to vary through the thickness of a sphere according to power law functions, Jabbari *et al*. (2013) carried out an analytical solution for the thermo-elastic analysis of a poro-piezo-FGM hollow sphere. They obtained the temperature distribution along the sphere thickness**,** and solved Navier equations analytically**,** using Legendre polynomials and Euler differential equations system to investigate the effect of graded indices, compressibility and porosity on mechanical and electrical quantities. Yang *et al*. (2014) presented an approximate elasticity solution for the bending analysis of simply supported or clamped transversely isotropic FG circular plates subjected to a concentrated force at the center of its upper face by extending England's method.

Wirowski *et al*. (2015) analyzed the dynamic behavior of FG annular plates resting on a two parameter elastic and heterogeneous material foundation using an averaged mathematical model. Sladek *et al*. (2015) considered the uncoupled thermo-elasticity theory and meshless local

Petrov-Galerkin method to investigate the bending of a porous piezoelectric cylinder under thermal loading.

The semi-analytical method which was originally proposed for free vibration analysis of generally laminated beams by Chen *et al*. (2004), is applicable to more complicated problems. This approach employs the state space method (SSM) to express exactly the plate behavior along the thickness direction**,** and the one dimensional differential quadrature (DQ) rule to approximate the radial variations of the parameters. Assuming exponentially distributed mechanical properties in the thickness direction and considering the 3D theory of elasticity, Behravan Rad and co-authors (2010, 2012a) discussed static behavior of FG circular and annular plates resting on linear elastic foundations under the effect of axisymmetric transverse load. Nie and Zhong (2007) analyzed the three dimensional free and forced vibration of FG circular plate with various boundary conditions. Alibeigloo and Simintan (2011) investigated the static response of the FG circular and annular plates embedded in piezoelectric layers. Jodaei (2014) reported the static behavior of functionally graded piezoelectric annular plates resting on a Pasternak type elastic foundation. Behravan Rad (2015) extracted a new differential equation to describe the normal interaction between gradient hybrid foundation-structure, and analyzed the thermoelastic behavior of the FG circular plates supported by unconventional hybrid foundation under asymmetric and non-uniform mechanical loads and uniform thermal load**,** on the basis of the classical thermo-elasticity theory.

Assuming the material properties to vary with an exponential law in both thickness and radial directions, Nie and Zhong (2007a) investigated the axisymmetric bending of 2D-FG circular and annular plates. Davoodi *et al*. (2012) demonstrated the free vibration problem of multi-directional FG circular and annular plates. Their work covers the effect of different parameters on natural frequencies and corresponding mode shapes. Tahouneh and Yas (2014) analyzed the free vibration of thick multidirectional FG annular sector plates under various boundary conditions. In other study, Yas and Moloudi (2015) used this method to make three-dimensional free vibration analysis of multi-directional functionally graded piezoelectric annular plates on a two parameter elastic foundation. Asgari (2015) considered the finite element and Genetic Algorithm methods to optimize the materials distribution in a thick hollow cylinder with finite length made of 2D-FGMs under steady-state thermo-mechanical loading. In a series of papers, Behravan Rad and co-authors (2012b, 2013a, b) developed a semi-analytical solution to demonstrate the static behavior of uniform and non-uniform multi-directional functionally graded circular and annular plates supported by uniform and variable elastic foundations under compound mechanical loads. The progresses in the mechanics of functionally graded materials and structures have been reviewed in Gupta and Talha (2015) and Swaminathan *et al*. (2015) in a detailed manner. The Development of various semi-analytical numerical methods in the mechanics of functionally graded elastic/piezoelectric plates and shells has been introduced in Wu and Liu (2016).

The literature search indicates that there is no work covering the three dimensional static analysis of variable thickness of two directional functionally graded porous material circular plate supported by a heterogeneous hybrid foundation including horizontal friction force and subjected to compound mechanical loads. Hence, present study is devoted to this problem and investigates the static behavior of the plate in un-drain condition. Inclined traction and concentrated force in the center of the plate are taken into account to propose a more general solution. In this work, the elastic coefficients of the plate material are assumed to be graded in the thickness and radial directions according to an exponential law. The formulations are based on the three-dimensional theory of the elasticity, and a semi-analytical approach is employed to solve the governing equations. The accuracy of the proposed method is validated by comparing the results are available in the literature. A convergence study is accomplished to demonstrate the rapid convergence of the proposed method and its capability to solve the governing equations of complicated problems. The effects of material properties gradient indices, loads ratio, thickness to radius ratio, foundation parameters, foundation friction coefficient, variations of compressibility and porosity on the displacements and stress components are intensively investigated.

The novelties of the present study may be outlined as follows:

1) Multi-directional functionally graded porous material is introduced.

2) A semi-analytical solution is extended for the static analysis of variable thickness of 2D functionally graded porous materials (FGPM) circular plate with complicated boundary conditions.

3) The model of structure-foundation interaction is developed by considering a horizontal friction force in contact surface of plate and foundation.

4) The effect of concentrated force at the center of solid circular plate is approximated by
considering a shear force uniformly distributed over the inner boundary of annular plate.

5) The effect of compressibility, porosity and foundation friction coefficient variations on the static behavior of variable thickness of 2D-FGPM circular plate is illustrated for the first time.

6) And last but not least, quite a new and interesting stress and deformation results for the
non-uniform2D-FGPM circular plate are presented.

7) The static response of multidirectional FG and Porous FG circular plates to compound mechanical loads are compared, for the first time.

2. Mathematical formulations

2.1 Problem description

Consider a continuously varying thickness bi-directional porous FGM circular plate with thickness (h_o) at the center and radius (a) resting on a gradient hybrid foundation and

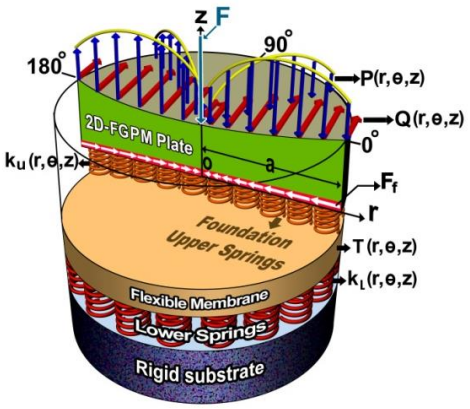

Fig. 1 Geometry of variable thickness of 2D Porous FG circular plate resting on a gradient hybrid foundation including friction force

subjected to compound mechanical loads, as shown in Fig. 1. The plate is clamped or simply supported at the circumferential edge. Its bottom surface is flat and attached to supporting medium. The thickness of the plate at upper surface varies along the radial direction by continues function $h(r)$. A cylindrical coordinate system (r, θ, z) whose origin o located at the center of bottom plane of the plate is employed to describe the displacement field.

The plate elastic constants, external loads and plate thickness variations are considered as follows

$$C_{ij}(r,z)=C_{ij}^{0}\exp\left[n_1\left(\frac{z}{h}\right)+n_2\left(\frac{r}{a}\right)\right] \tag{1}$$

i. Quadratic loads

$$P(r,\theta,z)=p_o\left[1+p_1\left(\frac{r}{a}\right)+p_2\left(\frac{r}{a}\right)^2\right]\cos(\theta),$$

$$Q(r,\theta,z)=q_o\left[1+q_1\left(\frac{r}{a}\right)+q_2\left(\frac{r}{a}\right)^2\right]\cos(\theta) \tag{2}$$

ii. Sinusoidal loads

$$P(r,\theta,z)=p_o\left[1+\lambda_1\sin\left(\pi\frac{r}{a}\right)\right]\cos(\theta)$$

$$Q(r,\theta,z)=q_o\left[1+\lambda_2\sin\left(\pi\frac{r}{a}\right)\right]\cos(\theta) \tag{3}$$

Exponential type thickness variation

$$h(r)=h_o\exp\left[\alpha_1\left(\frac{r}{a}\right)\right] \tag{4}$$

where C_{ij}^{0} is the elastic coefficients at the center of bottom surface of the plate, n_1, n_2 denote the parameters indicating the trends of the plate material properties gradient, p_o, q_o specify the values of external loads at the center of the plate, α_i, p_i, q_i, λ_i and i=1,2,3 characterize the plate geometry and external loads variation coefficients.

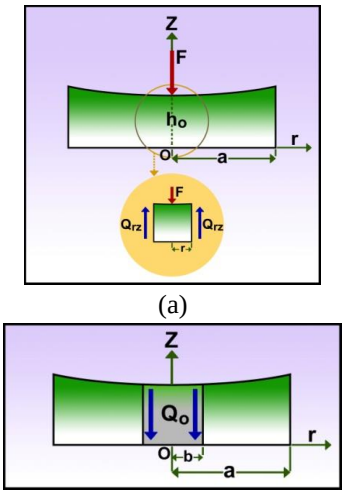

Fig. 2 Sketch of a non-uniform 2D porous FGM circular plate concentrically loaded

2.2 FGM circular plate with concentrated force at the center

Consider a porous FG circular plate subjected to a concentrated force F at the center with thickness $h(r)$ and radius a as shown in Fig. 2(a). The concentrated force can be approximated with resultant shearing force $Q_{rz}(r)$ at a distance r from the center of the plate. The following equation can be achieved from equilibrium in the z-direction.

$$Q_{rz}=\frac{F}{2\pi rh} \tag{5}$$

Now the FGPM circular plate can be replaced by an FGPM annular plate. Suppose the FGPM annular plate with a small inner radius b and resultant shearing force $Q_0=\frac{F}{2\pi b\,h(b)}$ uniformly distributed along the inner edge, as depicted in Fig. 2(b). The Eqs. (1) through (4) can be stated as

$$C_{ij}(r,z)=C_{ij}^{0}\exp\left[n_1\left(\frac{z}{h}\right)+n_2\left(\frac{r-b}{a-b}\right)\right] \tag{6a}$$

$$h(r)=h_o\exp\left[\alpha_1\left(\frac{r-b}{a-b}\right)\right] \tag{6b}$$

$$P(r,\theta,z)=p_o\left[1+p_1\left(\frac{r-b}{a-b}\right)+p_2\left(\frac{r-b}{a-b}\right)^2\right]\cos(\theta),$$

$$Q(r,\theta,z)=q_o\left[1+q_1\left(\frac{r-b}{a-b}\right)+q_2\left(\frac{r-b}{a-b}\right)^2\right]\cos(\theta) \tag{6c}$$

$$P(r,\theta,z)=p_o\left[1+\lambda_1\sin\left(\pi\frac{r-b}{a-b}\right)\right]\cos(\theta),$$

$$Q(r,\theta,z)=q_o\left[1+\lambda_2\sin\left(\pi\frac{r-b}{a-b}\right)\right]\cos(\theta) \tag{6d}$$

2.3 Derivation of governing equations

In the absence of body forces, the elastic equilibrium equations are

$$\begin{cases} \sigma_{r,r} + r^{-1}\tau_{r\theta,\theta} + \tau_{rz,z} + r^{-1}(\sigma_r - \sigma_\theta) = 0 \\ \tau_{r\theta,r} + r^{-1}\sigma_{\theta,\theta} + \tau_{\theta z,z} + 2r^{-1}\tau_{r\theta} = 0 \\ \tau_{rz,r} + r^{-1}\tau_{\theta z,\theta} + \sigma_{z,z} + r^{-1}\tau_{rz} = 0 \end{cases} \tag{7}$$

where σ_r, σ_θ, σ_z, τ_{rz}, $\tau_{r\theta}$ are the stress components and the comma denotes differentiation with respect to the indicated variable.

The displacements field is considered as (Nie and Zhang 2007)

$$\begin{cases} u(r,\theta,z) = u(r,z)\cos(\theta) \\ v(r,\theta,z) = v(r,z)\sin(\theta) \\ w(r,\theta,z) = w(r,z)\cos(\theta) \end{cases} \tag{8}$$

where u,v,w denote the displacement components in the r, θ and z directions.

The Cauchy's strain components are:

$$\begin{cases} \varepsilon_r = u(r,\theta,z)_{,r} \\ \varepsilon_\theta = r^{-1}v(r,\theta,z)_{,\theta} + r^{-1}u \\ \varepsilon_z = w(r,\theta,z)_{,z} \end{cases}$$

$$\begin{cases} \gamma_{rz} = u(r,\theta,z)_{,z} + w(r,\theta,z)_{,r} \\ \gamma_{\theta z} = r^{-1}w(r,\theta,z)_{,\theta} + v(r,\theta,z)_{,z} \\ \gamma_{r\theta} = r^{-1}u(r,\theta,z)_{,\theta} + v(r,\theta,z)_{,r} - r^{-1}v(r,\theta,z) \end{cases} \tag{9}$$

where ε_r, ε_θ, ε_z, γ_{rz}, $\gamma_{\theta z}$, $\gamma_{r\theta}$ denote the strain components.

The linear constitutive relations for a functionally graded porous material circular plate are as follows (Jabbari *et al*. 2013)

$$\begin{cases} \sigma_r = C_{11}\varepsilon_r + C_{12}\varepsilon_\theta + C_{13}\varepsilon_z - \gamma P, & \tau_{rz} = C_{44}\gamma_{rz} \\ \sigma_\theta = C_{21}\varepsilon_r + C_{22}\varepsilon_\theta + C_{23}\varepsilon_z - \gamma P, & \tau_{\theta z} = C_{55}\gamma_{\theta z} \\ \sigma_z = C_{31}\varepsilon_r + C_{32}\varepsilon_\theta + C_{33}\varepsilon_z - \gamma P, & \tau_{r\theta} = C_{66}\gamma_{r\theta} \end{cases} \tag{10}$$

where γ denotes the Biots coefficient of effective stress and P is the pore pressure. Other material properties for porous materials can be stated as

$$\begin{aligned} &P = (\psi - \gamma\varepsilon)\Phi, \quad \Phi = \frac{\lambda_u - \lambda}{\gamma^2}, \quad B = \frac{\lambda_u - \lambda}{\gamma\lambda_u}, \\ &\lambda_u = \lambda\left[1 + \frac{\gamma^2\lambda_f}{(1-\gamma)(\gamma - \phi_p)\lambda_f + \phi_p\lambda_f}\right] \end{aligned} \tag{11}$$

For fluid in un-drained condition (ψ=0) the first term of Eq. (11) leads to

$$P = -\Phi\gamma\varepsilon = -\gamma\Phi(\varepsilon_r + \varepsilon_\theta + \varepsilon_z) \tag{12}$$

where ψ, ε, Φ, λ_u, λ, λ_f, B, ϕ_p denote the variation of fluid content, volumetric strain, Biots Moduli, undrained bulk modulus, drained bulk modulus, bulk modulus of fluid, compressibility coefficient and porosity. Substituting Eq. (12) in to Eq. (10) leads to (Jabbari *et al*. 2013)

$$\begin{cases} \sigma_r = C_{11}^* u(r,\theta,z)_{,r} + C_{12}^* r^{-1}\left(v(r,\theta,z)_{,\theta} + u(r,\theta,z)\right) \\ \quad + C_{13}^* w(r,\theta,z)_{,z} \\ \sigma_\theta = C_{21}^* u(r,\theta,z)_{,r} + C_{22}^* r^{-1}\left(v(r,\theta,z)_{,\theta} + u(r,\theta,z)\right) \\ \quad + C_{23}^* w(r,\theta,z)_{,z} \\ \sigma_z = C_{31}^* u(r,\theta,z)_{,r} + C_{32}^* r^{-1}\left(v(r,\theta,z)_{,\theta} + u(r,\theta,z)\right) \\ \quad + C_{33}^* w(r,\theta,z)_{,z} \end{cases}$$

$$\begin{cases} \tau_{rz} = C_{44}\left(u(r,\theta,z)_{,z} + w(r,\theta,z)_{,r}\right) \\ \tau_{\theta z} = C_{55}\left(r^{-1}w(r,\theta,z)_{,\theta} + v(r,\theta,z)_{,z}\right) \\ \tau_{r\theta} = C_{66}\left(v(r,\theta,z)_{,r} - r^{-1}v(r,\theta,z) + r^{-1}u(r,\theta,z)_{,\theta}\right) \end{cases} \tag{13}$$

where

$$\begin{cases} C_{11}^* = C_{11} + \gamma^2\Phi, \quad C_{22}^* = C_{22} + \gamma^2\Phi, \\ C_{33}^* = C_{33} + \gamma^2\Phi \\ C_{12}^* = C_{12} + \gamma^2\Phi, \quad C_{13}^* = C_{13} + \gamma^2\Phi \end{cases} \tag{14}$$

In order to transform from physical domain to computational domain and to present more general results, the following non-dimensional parameters are introduced

$$\begin{aligned} &U = \frac{u(r,\theta,z)}{h(r)}, \quad V = \frac{v(r,\theta,z)}{h(r)}, \quad W = \frac{w(r,\theta,z)}{h(r)}, \quad \eta = \frac{r}{a}, \\ &\hbar = \frac{h_o}{a}, \quad \xi = \frac{z(r)}{h(r)}, \quad 0 \le \xi \le 1 \\ &\bar{C}_{ij}^0 = C_{ij}^*/C_{33}^* \;\; i,j = 1,2,3, \quad \bar{C}_{ij}^0 = C_{ij}/C_{33}^* \;\; i,j = 4,5,6, \\ &\Gamma = -Q_0/C_{44}^0, \quad \Gamma = \bar{\Gamma}\Gamma, \quad \bar{\Gamma} = 1 \\ &\sigma_\eta = \frac{\sigma_r}{Y}, \; \sigma_\Theta = \frac{\sigma_\theta}{Y}, \; \sigma_\xi = \frac{\sigma_z}{Y}, \; \tau_{\eta\xi} = \frac{\tau_{rz}}{Y}, \\ &\tau_{\Theta\xi} = \frac{\tau_{\theta z}}{Y}, \quad \tau_{\eta\Theta} = \frac{\tau_{r\theta}}{Y}, \; Y = 1\text{GPa} \end{aligned} \tag{15}$$

Taking into account the Eqs. (6)-(15), the normalized form of the governing differential equations of the plate in the framework of the uncoupled poro-elasticity theory are obtained as

$$\begin{aligned} U_{,\xi\xi} = &-\left(\frac{\bar{C}_{11}^0}{\bar{C}_{55}^0}\right)(\hbar)^2\chi_1^2\left\{U_{,\eta\eta} + \left(\frac{1}{\eta} + \frac{n_2}{1-b/a} + 2\chi_2\right)U_{,\eta}\right. \\ &\left. + \left[\left(\frac{1}{\eta} + \frac{n_2}{1-b/a}\right)\chi_2 + \chi_3 - \frac{1}{\eta^2}\right]U\right\} \\ &-\left(\frac{\bar{C}_{12}^0}{\bar{C}_{55}^0}\right)(\hbar)^2\chi_1^2\frac{n_2}{\eta(1-b/a)}U + \left(\frac{\bar{C}_{66}^0}{\bar{C}_{55}^0}\right)(\hbar)^2\chi_1^2\frac{1}{\eta^2}U \\ &-\left(\frac{\bar{C}_{11}^0}{\bar{C}_{55}^0}\right)(\hbar)^2\chi_1^2\frac{1}{\eta}\left[V_{,\eta} + \left(\chi_2 + \frac{n_2}{1-b/a}\right)V\right] \end{aligned}$$

$$+\left(\frac{\bar{C}_{22}^{0}}{\bar{C}_{55}^{0}}\right)(\hbar)^2\chi_1^2\frac{V}{\eta^2}-\left(\frac{\bar{C}_{66}^{0}}{\bar{C}_{55}^{0}}\right)(\hbar)^2\chi_1^2\left[\frac{1}{\eta}V_{,\eta}+\left(\frac{\chi_2}{\eta}-\frac{1}{\eta^2}\right)V\right]$$
$$-n_1\hbar\chi_1\left(W_{,\eta}+\chi_2 W\right)-n_1 U_{,\xi}$$
$$-\left(\frac{\bar{C}_{13}^{0}}{\bar{C}_{55}^{0}}\right)\hbar\chi_1\left[W_{,\eta\xi}+\left(\chi_2+\frac{n_2}{1-b/a}+\frac{1}{\eta}\right)W_{,\xi}\right]+$$
$$\left(\frac{\bar{C}_{23}^{0}}{\bar{C}_{55}^{0}}\right)\frac{\hbar\chi_1}{\eta}W_{,\xi}-\hbar\chi_1\left(W_{,\eta\xi}+\chi_2 W_{,\xi}\right) \qquad (16a)$$

$$V_{,\xi\xi}=\left(\frac{\bar{C}_{12}^{0}}{\bar{C}_{44}^{0}}\right)(\hbar)^2\frac{\chi_1^2}{\eta}\left(U_{,\eta}+\chi_2 U\right)+\left(\frac{\bar{C}_{22}^{0}}{\bar{C}_{44}^{0}}\right)(\hbar)^2\chi_1^2\frac{U}{\eta^2}$$
$$+\left(\frac{\bar{C}_{66}^{0}}{\bar{C}_{44}^{0}}\right)(\hbar)^2\chi_1^2\left\{\frac{1}{\eta}U_{,\eta}+\left[\frac{1}{\eta}\left(\chi_2+\frac{n_2}{1-b/a}\right)+\frac{1}{\eta^2}\right]U\right\}$$
$$+\left(\frac{\bar{C}_{22}^{0}}{\bar{C}_{44}^{0}}\right)(\hbar)^2\chi_1^2\frac{V}{\eta^2}-\left(\frac{\bar{C}_{66}^{0}}{\bar{C}_{44}^{0}}\right)(\hbar)^2\chi_1^2\left\{V_{,\eta\eta}+\left(2\chi_2+\frac{1}{\eta}+\frac{n_2}{1-b/a}\right)V_{,\eta}\right.$$
$$\left.+\left[\chi_2+\chi_3+\left(\chi_2-\frac{1}{\eta}\right)\left(\frac{n_2}{1-b/a}\right)-\frac{1}{\eta^2}\right]V\right\}$$
$$+n_1\hbar\chi_1\frac{W}{\eta}-n_1 V_{,\xi}+\frac{1}{\eta}\left(\frac{\bar{C}_{23}^{0}}{\bar{C}_{44}^{0}}\right)W_{,\xi} \qquad (16b)$$

$$W_{,\xi\xi}=-n_1\left(\frac{\bar{C}_{13}^{0}}{\bar{C}_{33}^{0}}\right)\hbar\chi_1\left[U_{,\eta}+\left(\chi_2+\frac{1}{\eta}\right)U\right]-n_1\left(\frac{\bar{C}_{23}^{0}}{\bar{C}_{33}^{0}}\right)\hbar\chi_1\frac{V}{\eta}$$
$$-\left(\frac{\bar{C}_{44}^{0}}{\bar{C}_{33}^{0}}\right)\hbar^2\chi_1^2\left\{W_{,\eta\eta}+\left(\frac{1}{\eta}+2\chi_2+\frac{n_2}{1-b/a}\right)W_{,\eta}\right.$$
$$\left.+\left[\chi_3+\chi_2\left(\frac{1}{\eta}+\frac{n_2}{1-b/a}\right)-\frac{1}{\eta^2}\right]W\right\}$$
$$-\left(\frac{\bar{C}_{13}^{0}}{\bar{C}_{33}^{0}}\right)\hbar\chi_1\left[U_{,\eta\xi}+\left(\chi_2+\frac{1}{\eta}\right)U_{,\xi}\right]-\left(\frac{\bar{C}_{55}^{0}}{\bar{C}_{33}^{0}}\right)\hbar\chi_1\left[U_{,\eta\xi}\right.$$
$$\left.+\left(\frac{n_2}{1-b/a}+\chi_2+\frac{1}{\eta}\right)U_{,\xi}\right]-\left(\frac{\bar{C}_{23}^{0}}{\bar{C}_{44}^{0}}\right)\hbar\chi_1\frac{V_{,\xi}}{\eta}-n_1 W_{,\xi} \qquad (16c)$$

where $\chi_1=\exp\left[\alpha_1\left(\frac{\eta-b/a}{1-b/a}\right)\right]$, $\chi_2=\frac{\alpha_1}{(1-b/a)}$, $\chi_3=\left(\frac{\alpha_1}{1-b/a}\right)^2$

2.4 Coupled effect of gradient hybrid elastic foundation

The gradient hybrid foundation model provided by Behravan Rad (2015) is employed in this study. It is assumed that, the proposed foundation model is perfect, attached to the plate, isotropic (T_r=T_θ=T), non-uniform and involves the horizontally distributed variable friction force in the radial direction. The considered model consists of a perfectly flexible membrane under constant tension T and two layers of independent axial springs with stiffnesses k_1, k_u as shown in Fig. 1. In the referred coordinate system, the distributed normal traction and associated horizontal friction force on the plate are expressed as follows

$$\Psi-\frac{1}{r}\frac{\partial}{\partial r}\left(r\frac{T}{k_l+k_u}\frac{\partial\Psi}{\partial r}\right)-\frac{1}{r^2}\frac{\partial}{\partial\theta}\left(\frac{T}{k_l+k_u}\frac{\partial\Psi}{\partial\theta}\right)=$$
$$\left(\frac{k_l k_u}{k_l+k_u}\right)w-\frac{1}{r}\frac{\partial}{\partial r}\left(r\frac{Tk_u}{k_l+k_u}\frac{\partial w}{\partial r}\right)-\frac{1}{r^2}\frac{\partial}{\partial\theta}\left(\frac{Tk_u}{k_l+k_u}\frac{\partial w}{\partial\theta}\right) \qquad (17)$$

$$F_f=\mu_f\,\Psi \qquad (18)$$

where Ψ denotes the foundation reaction per unit area and w is the lateral deflection of the bottom surface of the plate. k_1, T, k_u and μ_f, specify the hybrid foundation stiffnesses and foundation friction coefficient, respectively. Two types of radial variations of the foundation coefficients are considered in the present study.

i. Exponential type

$$\begin{cases} k_l(r,\theta,z)=k_{lo}\exp\left[f_1\left(\frac{r-b}{a-b}\right)\right]\cos(\theta) \\ T(r,\theta,z)=T_o\exp\left[f_2\left(\frac{r-b}{a-b}\right)\right]\cos(\theta) \\ k_u(r,\theta,z)=k_{uo}\exp\left[f_3\left(\frac{r-b}{a-b}\right)\right]\cos(\theta) \end{cases} \qquad (19a)$$

ii. Sinusoidal type

$$\begin{cases} k_l(r,\theta,z)=K_{lo}\left[1+\mu_1\sin\left(\pi\frac{r-b}{a-b}\right)\right]\cos(\theta) \\ T(r,\theta,z)=T_o\left[1+\mu_2\sin\left(\pi\frac{r-b}{a-b}\right)\right]\cos(\theta) \\ k_u(r,\theta,z)=K_{uo}\left[1+\mu_3\sin\left(\pi\frac{r-b}{a-b}\right)\right]\cos(\theta) \end{cases} \qquad (19b)$$

where k_{1o} (N/m^3), T_o (N/m) and k_{uo} (N/m^3) are the elastic coefficients of hybrid foundation at the center of bottom surface of the plate and f_i, μ_i and i=1,2,3 characterize the foundation inhomogeneity exponents.

3. The solution technique

In order to study the static behavior of the FGPM circular plate, the expressed differential equations in Eq. (16) is solved utilizing a semi-analytical method. By employing this method, the mathematical model of proposed problem is transformed to computational domain and then by implementing the edge and the boundary conditions, the established linear eigenvalue system from state variables at all sample points is solved. Finally, the displacements and stress components of the plate under compound mechanical tractions are obtained.

3.1 DQM procedure and its application

Differential quadrature (DQ) method is a numerical technique whit fast rate of convergence and less required grid points in the solution domain. This method is dominated by these two features. DQ method divides the continuous domain in to a set of discrete points and replaces the derivative of an arbitrary unknown function with the weighted linear summation of the function values in the

whole domain. According to this method, the nth-order derivative of a continuous function $g(r)$ defined in an interval $r\in[0,1]$, with respect to argument r at an arbitrary given point r_i can be approximated as follows (Jodaei 2014, Behravan Rad 2015)

$$\frac{\partial^{(n)} g(r_i)}{\partial r^n} = \sum_{j=1}^{N} A_{ij}^{(n)} g(r_j)$$
$$i = 1,2,\cdots,N \quad \text{and} \quad n = 1,2,\cdots,N-1 \tag{20}$$

where $A_{ij}^{(n)}$ is the weighting coefficients matrix of the nth-derivative determined by the coordinates of the sample points r_i and N is the number of the grid points in the radial direction.

There are different ways to estimate the weighting coefficient matrix, because different functions may be considered as test functions. In this study a set of Lagrange interpolation polynomials are employed as test functions to procure the weighting coefficients, and to achieve more accuracy, the non-uniform grid spacing is adopted. Explicit expressions of the first and second derivatives of the weighted coefficients matrices and also criterion to adopt non-uniformly spaced grid points are as follows (Behravan Rad 2012a). The first order derivative of the weighting coefficients matrix is

$$\begin{cases} A_{ik} = \dfrac{\prod_{j=1, j\neq i}^{N} (r_i - r_j)}{(r_i - r_k) \prod_{j=1, j\neq k}^{N} (r_k - r_j)}, \\ \qquad i \neq k, \quad i,k = 1,2,3,\cdots,N \\ A_{ii} = -\sum_{j=1, j=i}^{N} A_{ij}, \\ i = k, \quad i = 1,2,3,\cdots,N \end{cases} \tag{21}$$

Furthermore, for the second-order derivative, the weighting coefficients matrix may be approximated by the following relations.

$$\begin{cases} A_{ik}^{(2)} = 2\left(A_{ii} A_{ik} - \dfrac{A_{ik}}{r_i - r_k} \right), \\ \qquad i \neq k \quad , \quad i,k = 1,2,3,\cdots,N \\ A_{ii}^{(2)} = -\sum_{j=1, j=i}^{N} A_{ij}^{(2)} \quad , \\ \qquad i = k \quad , \quad i = 1,2,3,\cdots,N \end{cases} \tag{22}$$

To achieve the more reliable and accurate results, the Chebyshev-Gauss-Lobatto criterion is used as

$$r_i = \frac{1}{2}\left\{1 - \cos\left[\frac{(i-1)\pi}{N-1}\right]\right\}(a-b) + b$$
$$i = 1,2,3,\cdots,N \tag{23}$$

The partial derivatives of the unknown displacements U,V,W with respect to η appeared in Eq. (16) after applying the DQ rule at an arbitrary sample point η_i can be expressed as

$$U,_{\eta}\Big|_{\eta=\eta i} = \sum_{j=1}^{N} A_{ij} U_j \quad , \quad V,_{\eta}\Big|_{\eta=\eta i} = \sum_{j=1}^{N} A_{ij} V_j,$$

$$W,_{\eta}\Big|_{\eta=\eta i} = \sum_{j=1}^{N} A_{ij} W_j \quad , \quad U,_{\eta\eta}\Big|_{\eta=\eta i} = \sum_{j=1}^{N} A_{ij}^{(2)} U_j$$

$$V,_{\eta\eta}\Big|_{\eta=\eta i} = \sum_{j=1}^{N} A_{ij}^{(2)} V_j \quad , \quad W,_{\eta\eta}\Big|_{\eta=\eta i} = \sum_{j=1}^{N} A_{ij}^{(2)} W_j$$

$$U,_{\eta\xi}\Big|_{\eta=\eta i} = \sum_{j=1}^{N} A_{ij} U_{,\xi j} \quad , \quad V,_{\eta\xi}\Big|_{\eta=\eta i} = \sum_{j=1}^{N} A_{ij} V_{,\xi j}$$

$$W,_{\eta\xi}\Big|_{\eta=\eta i} = \sum_{j=1}^{N} A_{ij} W_{,\xi j} \tag{24}$$

3.2 Boundary conditions

The following boundary conditions are considered in this study

Clamped:

$$u(r,\theta,z) = 0, \quad v(r,\theta,z) = 0, \quad w(r,\theta,z) = 0,$$
$$\text{at} \quad r = a \tag{25}$$

Simply supported:

$$\sigma_r(r,\theta,z) = 0, \quad v(r,\theta,z) = 0, \quad w(r,\theta,z) = 0,$$
$$\text{at} \quad r = a \tag{26}$$

On the inner edge:

$$\sigma_r(r,\theta,z) = 0, \quad \tau_{rz}(r,\theta,z) = -Q_0, \quad \tau_{\theta z}(r,\theta,z) = 0,$$
$$\text{at} \quad r = b \tag{27}$$

The bottom and top surfaces boundary conditions are

$$\sigma_z = \Psi(r,\theta,z), \ \tau_{z\theta} = 0, \ \tau_{rz} = F_f, \quad \text{at} \quad z = 0 \tag{28}$$

$$\sigma_z = -P(r,\theta,z), \tau_{z\theta} = Q(r,\theta,z), \ \tau_{rz} = 0, \text{at} \, z = h \tag{29}$$

The associated edge conditions in discretized points can be written as follows

Clamped:

$$U_N = 0, \quad V_N = 0, \quad W_N = 0, \quad \text{at} \quad \eta = 1 \tag{30}$$

Simply supported:

$$\sigma_{\eta N} = 0, \quad V_N = 0, \quad W_N = 0, \quad \text{at} \quad \eta = 1 \tag{31}$$

On the inner edge:

$$\sigma_{\eta 1} = 0, \ \tau_{\eta\xi 1} = -Q_0, \ \tau_{\Theta\xi 1} = 0, \quad \text{at} \quad \eta = b/a \tag{32}$$

The discretized forms of the boundary conditions at the lower and upper surfaces of the plate, Eqs. (28) and (29) can be written as

At $\xi = 0$,

$$\left(U,_{\xi}\right)_i + \hbar \chi_{1i}\left(\sum_{j=1}^{N} A_{ij} W_j + \chi_{2i} W_i\right) = F_f,$$
$$\left(V,_{\xi}\right)_i - \hbar \frac{\chi_{1i} \cot g(\theta)}{\eta_i} W_i = 0 \tag{33}$$
$$\left(W,_{\xi}\right)_i + \frac{\overline{C}_{13}^{0}}{\overline{C}_{33}^{0}} \hbar \chi_{1i} \left[\sum_{j=1}^{N} A_{ij} U_j + \left(\chi_{2i} + \frac{1}{\eta_i}\right) U_i + \frac{\text{tg}(\theta)}{\eta_i} V_i \right] = \Omega$$

$$\Omega=\left[1+\left(\frac{1}{a}\right)^2\frac{1}{\eta_i^{\,2}}\frac{\chi_{11i}\left(\chi_{4i}+\chi_{6i}\right)-\chi_{5i}\left(\chi_{10i}+\chi_{12i}\right)}{\left(\chi_{4i}+\chi_{6i}\right)^2}\mathrm{tg}(\theta)+\frac{\chi_{5i}}{\chi_{4i}+\chi_{6i}}\right]$$

$$\overline{\Psi}_i-\left(\frac{1}{a}\right)^2\frac{\chi_{5i}}{\chi_{4i}+\chi_{6i}}\sum_{j=1}^{N}A_{ij}^{(2)}\overline{\Psi}_j$$

$$-\left(\frac{1}{a}\right)^2\frac{1}{\chi_{4i}+\chi_{6i}}\left(\frac{\chi_{5i}}{\eta_i}+\frac{\chi_{8i}\left(\chi_{4i}+\chi_{6i}\right)-\chi_{5i}\left(\chi_{7i}+\chi_{9i}\right)}{\chi_{4i}+\chi_{6i}}\right)\sum_{j=1}^{N}A_{ij}\overline{\Psi}_j=$$

$$\left(\frac{\chi_{1i}\chi_{4i}\chi_{6i}}{\chi_{4i}+\chi_{6i}}\right)\frac{h_0}{C_{33}^{*}\exp\left[n_2\left(\frac{\eta_i-b/a}{1-b/a}\right)\right]}W_i-\left(\frac{1}{a}\right)^2\frac{h_0}{\eta_i}$$

$$\frac{1}{C_{33}^{*}\exp\left[n_2\left(\frac{\eta_i-b/a}{1-b/a}\right)\right]}\left(\frac{\chi_{1i}\chi_{5i}\chi_{6i}}{\chi_{4i}+\chi_{6i}}\right)\left(\sum_{j=1}^{N}A_{ij}W_j+\chi_{2i}W_i\right)$$

$$-\left(\frac{1}{a}\right)^2\frac{h_0}{C_{33}^{*}\exp\left[n_2\left(\frac{\eta_i-b/a}{1-b/a}\right)\right]}$$

$$\left(\frac{\chi_{1i}\left(\chi_{8i}\chi_{6i}+\chi_{9i}\chi_{5i}\right)\left(\chi_{4i}+\chi_{6i}\right)-\chi_{1i}\chi_{5i}\chi_{6i}\left(\chi_{7i}+\chi_{9i}\right)}{\left(\chi_{4i}+\chi_{6i}\right)^2}\right)\left(\sum_{j=1}^{N}A_{ij}W_j+\chi_{2i}W_i\right)$$

$$-\left(\frac{1}{a}\right)^2\frac{h_0}{C_{33}^{*}\exp\left[n_2\left(\frac{\eta_i-b/a}{1-b/a}\right)\right]}$$

$$\left(\frac{\chi_{1i}\chi_{5i}\chi_{6i}}{\chi_{4i}+\chi_{6i}}\right)\left(\sum_{j=1}^{N}A_{ij}^{(2)}W_j+2\chi_{2i}\sum_{j=1}^{N}A_{ij}W_j+\chi_{3i}W_i\right)$$

$$\overline{\Psi}=\Psi/C_{33}^{*}\exp\left[n_2\left(\frac{\eta_i-b/a}{1-b/a}\right)\right] \text{ and}$$

i. Exponential type

$$\chi_{4i}=k_{lo}\exp\left[f_1\left(\frac{\eta_i-b/a}{1-b/a}\right)\right]\cos(\theta),$$

$$\chi_{5i}=T_o\exp\left[f_2\left(\frac{\eta_i-b/a}{1-b/a}\right)\right]\cos(\theta),$$

$$\chi_{6i}=k_{uo}\exp\left[f_3\left(\frac{\eta_i-b/a}{1-b/a}\right)\right]\cos(\theta),$$

$$\chi_{7i}=\chi_{4i}\times f_1/(1-b/a),$$

$$\chi_{8i}=\chi_{6i}\times f_2/(1-b/a),$$

$$\chi_{9i}=\chi_{8i}\times f_3/(1-b/a),$$

$$\chi_{10i}=-k_{lo}\exp\left[f_1\left(\frac{\eta_i-b/a}{1-b/a}\right)\right]\sin(\theta),$$

$$\chi_{11i}=-T_o\exp\left[f_2\left(\frac{\eta_i-b/a}{1-b/a}\right)\right]\sin(\theta),$$

$$\chi_{12i}=-k_{uo}\exp\left[f_3\left(\frac{\eta_i-b/a}{1-b/a}\right)\right]\sin(\theta)$$

ii. Sinusoidal loads

$$\chi_{4i}=K_{lo}\left[1+\mu_1\sin\left(\pi\frac{\eta_i-b/a}{1-b/a}\right)\right]\cos(\theta),$$

$$\chi_{5i}=T_o\left[1+\mu_2\sin\left(\pi\frac{\eta_i-b/a}{1-b/a}\right)\right]\cos(\theta),$$

$$\chi_{6i}=K_{uo}\left[1+\mu_3\sin\left(\pi\frac{\eta_i-b/a}{1-b/a}\right)\right]\cos(\theta),$$

$$\chi_{7i}=K_{lo}\frac{\mu_1\pi}{1-b/a}\left[\cos\left(\pi\frac{\eta_i-b/a}{1-b/a}\right)\right]\cos(\theta),$$

$$\chi_{8i}=T_o\frac{\mu_2\pi}{1-b/a}\left[\cos\left(\pi\frac{\eta_i-b/a}{1-b/a}\right)\right]\cos(\theta),$$

$$\chi_{9i}=K_{uo}\frac{\mu_3\pi}{1-b/a}\left[\cos\left(\pi\frac{\eta_i-b/a}{1-b/a}\right)\right]\cos(\theta),$$

$$\chi_{10i}=-K_{lo}\left[1+\mu_1\sin\left(\pi\frac{\eta_i-b/a}{1-b/a}\right)\right]\sin(\theta),$$

$$\chi_{11i}=-T_o\left[1+\mu_2\sin\left(\pi\frac{\eta_i-b/a}{1-b/a}\right)\right]\sin(\theta),$$

$$\chi_{12i}=-K_{uo}\left[1+\mu_3\sin\left(\pi\frac{\eta_i-b/a}{1-b/a}\right)\right]\sin(\theta)$$

At $\xi=1$,

$$\left(U,\xi\right)_i+\hbar\chi_{1i}\left(\sum_{j=1}^{N}A_{ij}W_j+\chi_{2i}W_i\right)=0$$

$$\left(V,\xi\right)_i-\hbar\frac{\chi_{1i}\cot g(\theta)}{\eta_i}W_i=$$

$$\frac{Q_i}{\overline{C}_{44}^{0}C_{33}^{*}\exp\left[n_1+n_2\left(\frac{\eta_i-b/a}{1-b/a}\right)\right]}$$

$$\left(W,\xi\right)_i+\frac{\overline{C}_{13}^{0}}{\overline{C}_{33}^{0}}\hbar\chi_{1i}\left[\begin{array}{l}\sum_{j=1}^{N}A_{ij}U_j+\left(\chi_{2i}+\frac{1}{\eta_i}\right)U_i\\ +\frac{\mathrm{tg}(\theta)}{\eta_i}V_i\end{array}\right]= \quad (34)$$

$$\frac{-P_i}{C_{33}^{*}\exp\left[n_1+n_2\left(\frac{\eta_i-b/a}{1-b/a}\right)\right]}$$

3.3 The state space method

Assembling of governing equations appeared in Eq. (19) in a state space notation at all discrete points gives the global state equation in a matrix form as

$$\left\{\Delta_i(\xi)\right\}_{,\xi}=\left[D_i\right]\left\{\Delta_i(\xi)\right\}+\left[B_i\right]\left\{L_i(\xi)\right\} \quad (35)$$

Here, $\Delta_i(\xi)^T=\left[U_i \quad V_i \quad W_i \quad U_{,\xi i} \quad V_{,\xi i} \quad W_{,\xi i}\right]$,

Table 1 Mechanical constants (PZT-4)

FGM constants (GPa)					
C_{11}=C_{22}	C_{12}=C_{21}	C_{13}=C_{23}	C_{33}	C_{44}=C_{55}	C_{66}
139	78	74	115	25.6	30.5
Poro constants					
γ	λ_u (GPa)	λ (GPa)	λ_f (GPa)	B	ϕ_p
0.27	41	35	35e−6	0.45	0.02

$\mathrm{L_i}(\xi)^{\mathrm{T}}=\left[0 \quad 0 \quad 0 \quad \overline{\Gamma_i} \quad 0 \quad 0\right]$ are the global state and concentrated load vectors along the plate thickness at the level of ξ, respectively. D_i, B_i are the coefficient matrices at sample points. The details of these matrices are demonstrated in appendix 1.

By applying boundary conditions at edges, the Eq. (35) leads to the following equation

$$\left[\Delta_{ei}(\xi)\right]_{,\xi}=\left[\mathrm{D_{ei}}\right]\left[\Delta_{ei}(\xi)\right]+\left[\mathrm{B_{ei}}\right]\left[\mathrm{L_{ei}}(\xi)\right] \quad (36)$$

where the subscript 'e' denotes the modified matrix or unknown vector taking account of the edge conditions.

According to the rules of matrix operation, the general solution to Eq. (36) is

$$\Delta_{ei}(\xi)=\exp\left(\xi \mathrm{D_{ei}}\right)\Delta_{ei}(0)+\mathrm{H}_{\xi} \quad (37)$$

where the term H_{ξ} is the concentrate load vector defined by

$$\mathrm{H}_{\xi}=\int_0^{\xi}\exp\left((\xi-\tau)\mathrm{D_e}\right)\mathrm{B_e}(\tau)\,\mathrm{L}(\tau)\,\mathrm{d}\tau \quad (38)$$

The recent integral is implemented via numerical quadrature in the present study. Eq. (37) establishes the transfer relations from the state vector on the bottom surface to that at an arbitrary plane ξ of the plate by the exponential matrix of exp(ξD_{ei}). Setting ξ=1 in Eq. (38) gives

$$\Delta_{ei}(1)=\exp\left(\mathrm{D_{ei}}\right)\Delta_{ei}(0)+\mathrm{H}_1 \quad (39)$$

where exp(D_{ei}) is the global transfer matrix and H_1 is obtained by setting the upper bound of integration to unity in Eq. (38). $\Delta_{ei}(1)$, $\Delta_{ei}(0)$ are the values of the state variables at the upper and lower planes of the plate, respectively.

Taking into account the state of tractions presented in Eqs. (33), (34), the Eq. (39) can be derived in the form of algebraic equations as follows

$$\mathrm{M}\,\mathrm{X}=\mathrm{Q} \quad (40)$$

where M is a 6(N-1)×6(N-1) matrix, Q is a mechanical traction vector and

$$\mathrm{X}^{\mathrm{T}}=\left[\mathrm{U_i}(0) \quad \mathrm{V_i}(0) \quad \mathrm{W_i}(0) \quad \mathrm{U_i}(1) \quad \mathrm{V_i}(1) \quad \mathrm{W_i}(1)\right],$$

$$(\mathrm{i}=2,3,\cdots,N-1) \quad (41)$$

By solving Eq. (40), all state parameters at ξ=0, ξ=1 are obtained. Then, the Eqs. (36) and (13) are used to calculate the displacements and stress components at inner points of FGPM circular plate.

4. Numerical results and discussions

This section deals with the semi-analytical based numerical results for the static response of clamped and simply supported plates resting on a radially graded hybrid foundation to compound mechanical tractions. In this regard, two types of parametric studies are considered.

1. Parametric study for static behaviour in the absence of foundation friction force (μ_f=0)

2. Parametric study for static behaviour in the presence of foundation friction force (μ_f≠0)

The considered plates in the examples are assumed to be composed of PZT-4 at the center of lower surface of the plates. To extract the numerical results, the following material constants (listed in Table1), boundary conditions and other parameters are considered.

$$\tau_{rz}=\mathrm{F_f}\,,\sigma_z=\Psi\left(\mathrm{r},\theta,\mathrm{z}\right),\ \tau_{\theta z}=0,\quad \text{at}\ \ \xi=0 \quad (42a)$$

$$\tau_{rz}=0,\ \sigma_z=-1\mathrm{GPa}\,,\tau_{\theta z}=1\,\mathrm{GPa}\,,\quad \text{at}\ \ \xi=1 \quad (42b)$$

$$\mathrm{a}=1.0\,\mathrm{m}\,,\hbar=0.03\,,\mathrm{b}=0.002\,\mathrm{m}\,,\alpha_1=0.1,$$
$$\mathrm{f}_1=\mathrm{f}_2=\mathrm{f}_3=0.1,\mathrm{k_{lo}}=\mathrm{k_{uo}}=1\mathrm{GN/m}^3,\mathrm{T_o}=1\mathrm{GN/m}\,,$$
$$\mathrm{p}_0=\mathrm{q}_0=1,\ \mathrm{p}_1=\mathrm{p}_2=\mathrm{q}_1=\mathrm{q}_2=0.1,\quad \mathrm{F}=1\mathrm{KN}\,,\ \mu_{\mathrm{f}}=0.8 \quad (42c)$$

4.1 Parametric study for static behavior in the absence of foundation friction force (μ_f=0)

This section provides some numerical examples for the expressed problem. In this regard, the first example is devoted to verification purposes, the next example is conducted to convergence study of the presented approach and the other examples contain new results. In the plots, the effects of material heterogeneity indices, hybrid foundation coefficients, loads ratio, foundation graded indices; compressibility coefficient and porosity of the structure on the elastic field components are investigated.

Example 1: As a verification example, a uniform simply supported FG circular plate subjected to a concentrated force at the center of the plate considered previously by Yang *et al*. (2014) is reexamined. For the ease of comparison with this reference, the same problem is considered.

The validity and accuracy of the present method is investigated by solving the dimensionless deflection of the simply supported circular plate at a location η=(a−b)/2 with different thickness-to-radius ratios and gradient indices n_1. Comparisons of the present semi-analytical results and Yang's analytical results are shown on Table 2. The difference tolerance is taken to be 0.0005 and a good accuracy can be observed between the present numerical results and the Yang's analytical results. It is clear that the difference between the results of this study and the results of Yang's method may be expected, because the nature of solution methods is different. Unless otherwise stated, the thickness variation of the plate is exponential type in the next examples.

Table 2 Dimensionless deflection of simply supported circular plate at bottom plane and η=0.5

n_1	h/a=0.1		h/a=0.15		h/a=0.2	
	present	Yang *et al*. (2014)	present	Yang *et al*. (2014)	present	Yang *et al*. (2014)
−2	−0.1125	−0.1120	−0.0061	−0.0058	−0.0073	−0.0069
0	−0.0404	−0.0401	−0.0023	−0.0021	−0.0026	−0.0025
2	−0.0154	−0.0152	−0.0009	−0.0008	−0.0011	−0.0009

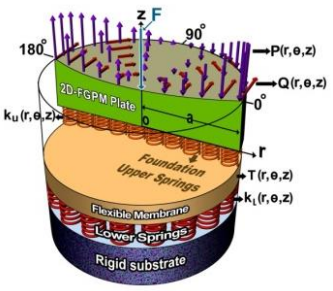

Fig. 3 Geometry of variable thickness of 2D Porous FG circular plate resting on a gradient hybrid foundation without friction force

Table 3 Convergence of the DQ method, w vs. N for clamped 2D-FGPM circular plate

		N								
		3	5	7	9	11	13	15	17	19
n_1	0.5	−0.423	−0.429	−0.435	−0.451	−0.451	−0.452	−0.450	−0.451	−0.451
=	1	−0.122	−0.127	−0.125	−0.124	−0.124	−0.125	−0.124	−0.124	−0.125
n_2	1.5	−0.046	−0.049	−0.047	−0.047	−0.047	−0.048	−0.047	−0.047	−0.047

Table 4 Convergence of the DQ method, σ_ξ vs. N for simply supported 2D-FGPM circular plate

		N								
		3	5	7	9	11	13	15	17	19
	0.5	-0.711	-0.751	-0.836	-0.863	-0.863	-0.863	-0.864	-0.863	-0.864
n_1=n_2	1	-0.445	-0.546	-0.789	-0.802	-0.803	-0.804	-0.802	-0.802	-0.803
	1.5	-0.258	-0.584	-0.649	-0.659	-0.658	-0.659	-0.659	-0.659	-0.658

Example 2: In order to assess the convergence of the proposed approach, non-uniform 2D-FGPM clamped and simply supported circular plates resting on radially graded hybrid foundation (exponential type variation) and subjected to asymmetric and quadratic type transverse and in-plane loads without horizontal friction force, as shown in Fig. 3 are considered. The boundary conditions and geometric parameters are the same as those in Eq. (45). The effect of the number of the selected sample points on the convergence of the dimensionless transverse deflection W and dimensionless transverse normal stress σ_ξ at a location η=(a−b)/2, θ=60° and ξ=0.5 are presented in Tables 3-4. From the tables, it can be seen that W_0 and σ_ξ approaches asymptotically to a specific value as the number of the discretization points increases beyond 9. Hence, present formulation converges with a high rate. In the present research, nine non-uniformly spaced, discretization points are adopted and all plots shown henceforth are obtained according to these sample points.

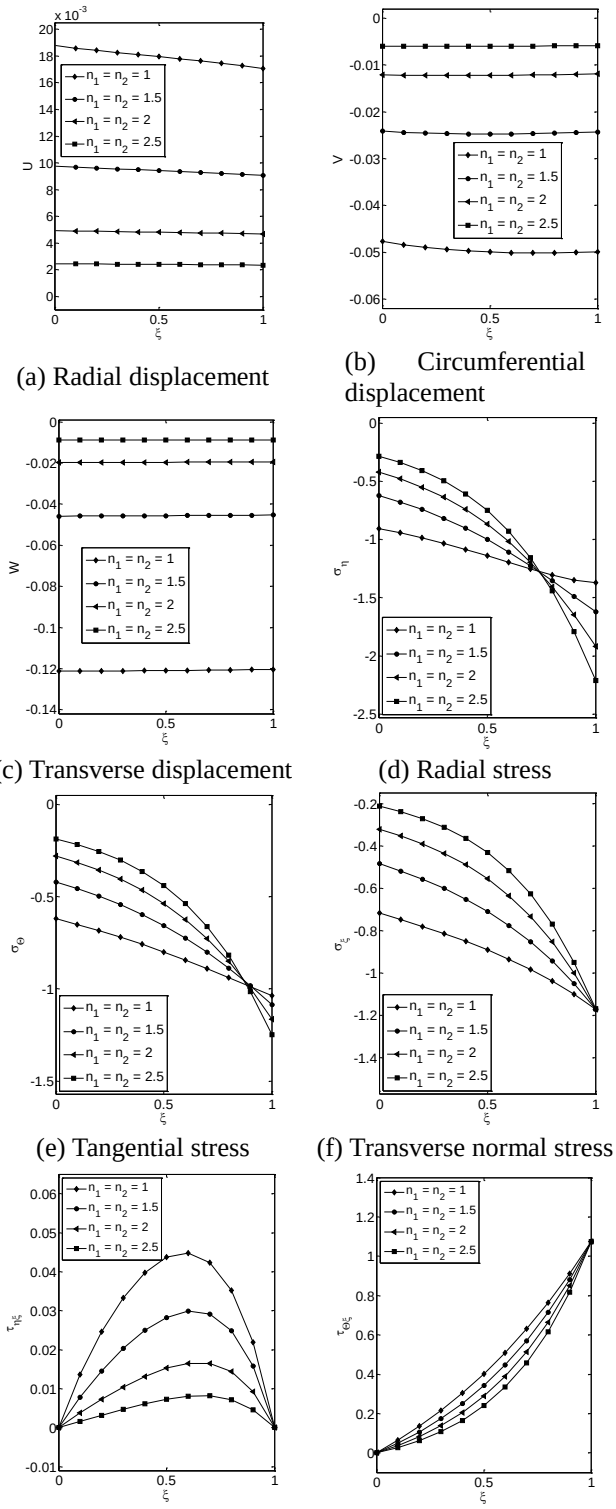

(a) Radial displacement (b) Circumferential displacement

(c) Transverse displacement (d) Radial stress

(e) Tangential stress (f) Transverse normal stress

(g) Transverse shear stress (h) Transverse shear stress

Fig. 4 Effect of the material heterogeneity indices on displacements and stress components of a clamped circular plate at location η=(a−b)/2 and θ=π/3

Example 3: In the present example, a parametric study is performed to illustrate the static behavior of non-uniform 2D-FGPM clamped circular plate resting on radially graded

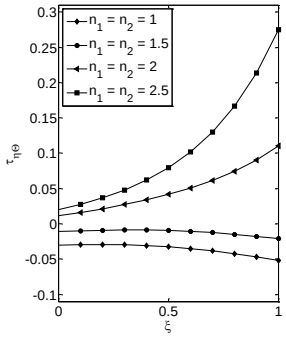

(i) Tangential shear stress

Fig. 4 Continued

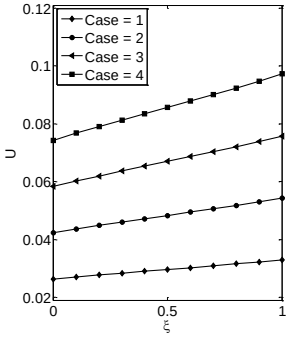

(a) Radial displacement

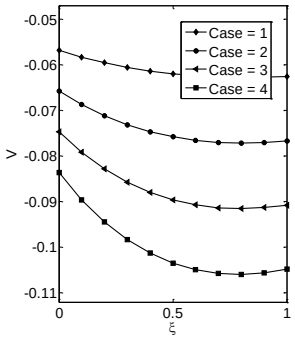

(b) Circumferential displacement

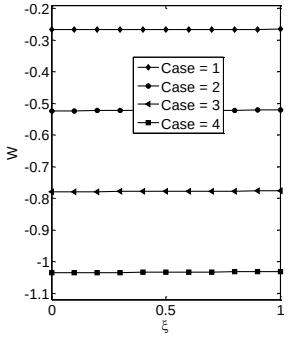

(c) Transverse displacement

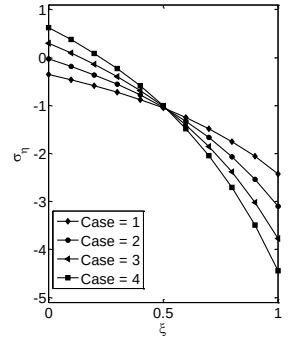

(d) Radial stress

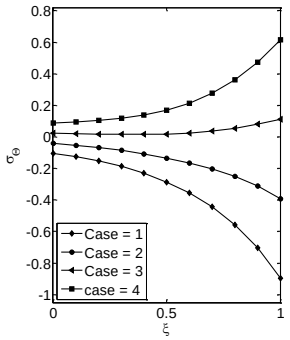

(e) Tangential stress

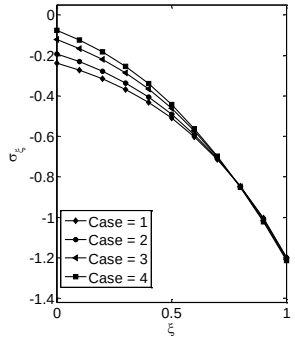

(f) Transverse normal stress

Fig. 5 Influence of the loads ratio on variation of mechanical entities across the plate thickness for a clamped circular plate at section η=(a−b)/2 and θ=π/6

hybrid foundation. The geometric parameters and boundary conditions are the same as those in Example 2. The results for the influence of different parameters (e.g., material

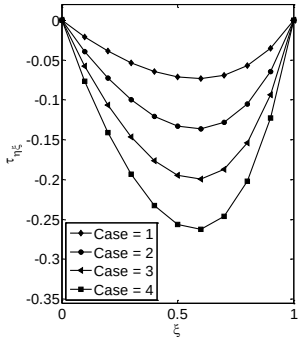

(g) Transverse shear stress

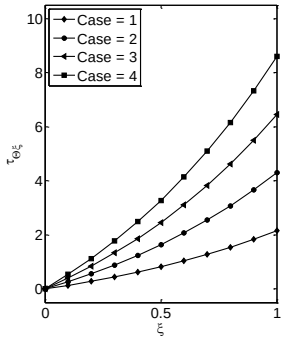

(h) Transverse shear stress

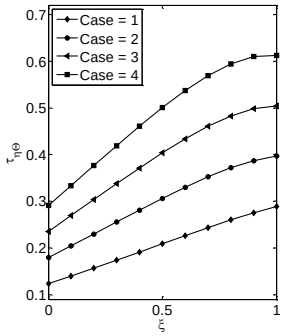

(i) Tangential shear stress

Fig. 5 Continued

heterogeneity graded indices, loads ratio and trends of foundation stiffness variations) on elastic field components are plotted in Figs. 4 to 6.

Fig. 4 depicts the influence of elastic graded indices on distributions of displacements and stresses along the thickness direction for a non-uniform 2D-FGPM solid circular plate at a location η=(a−b)/2, θ=60° under prescribed loading. Four different material graded indices are considered in this examination n_1=n_2=1, 1.5, 2, 2.5. The gradient indices increase cause to decrease U, V and W through the thickness of the plate. Moreover, as the Figs. 4 (a), (b) and (c) show, the distribution of displacements transforms to a monotonic distribution with increasing the gradient indices. As the Figs. 4 (b), (d) and (e) show, the distribution of circumferential displacement, in-plane radial and tangential stresses (σ_η, σ_Θ) along the thickness are more affected by the change of material gradient indices. As the Fig. 4(f) shows, the transverse normal stress σ_ξ is slightly increased through the thickness direction and converges to given boundary conditions at upper surface of the plate. It is clear from figure that shear stresses ($\tau_{\eta\xi}$, $\tau_{\Theta\xi}$) satisfy fully the given boundary conditions, and the pick value of the stress $\tau_{\eta\xi}$ decreases as n_1, n_2 increase. Moreover, the plate becomes stiffer for higher values of heterogeneity indices and the distribution of stress $\tau_{\eta\xi}$ converges to linear distribution, which is the characteristic of thin and stiffer plate. As the Fig. 3(h) shows, the stress $\tau_{\Theta\xi}$ is slightly decreased at the overall thickness of the plate and converges to given tangential load at top plane of the plate. Fig. 4(i) shows that the distribution of shear stress $\tau_{\eta\Theta}$ through the thickness direction decreases as n_1, n_2 increase.

Fig. 5 presents the effect of various loads ratio on the displacements and stress components of the plate at a

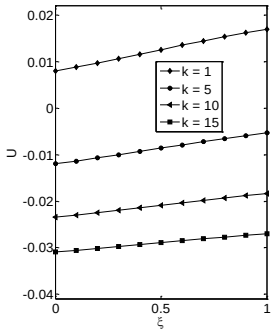

(a) Radial displacement

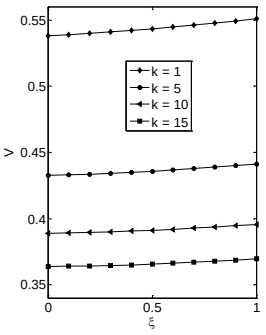

(b) Circumferential displacement

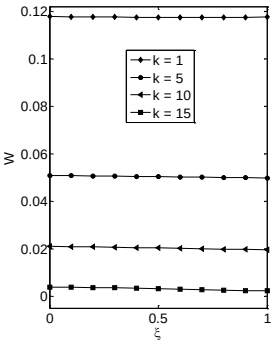

(c) Transverse displacement

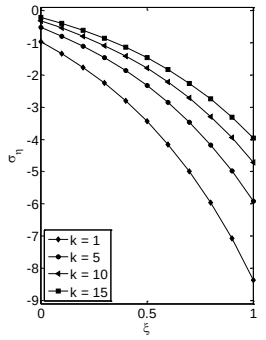

(d) Radial stress

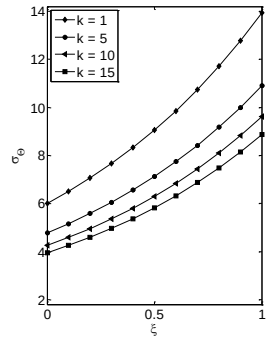

(e) Tangential stress

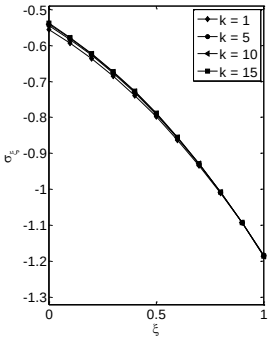

(f) Transverse normal stress

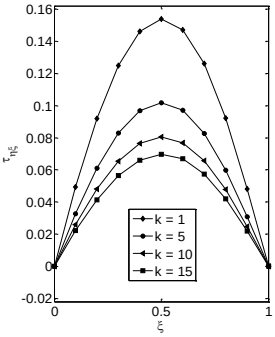

(g) Transverse shear stress

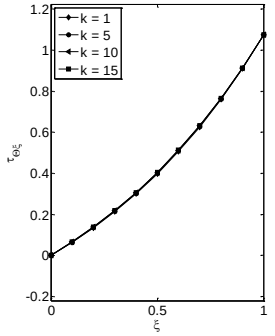

(h) Transverse shear stress

Fig. 6 Effect of the foundation coefficients variations on mechanical entities at location η=(a−b)/2 and θ=π/6 for a clamped circular plate supported by a gradient hybrid foundation

location θ=60° and η=(a−b)/2 with gradient indices n_1=n_2=1. Four sets of loads ratio are considered in this examination as follows:

Case 1: $q_0/p_0 = 2$, $q_0/F = 37.7$,

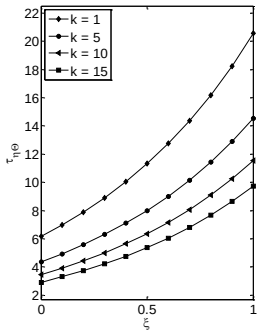

(i) Tangential shear stress

Fig. 6 Continued

Case 2: $q_0/p_0 = 4$, $q_0/F = 150.7$,

Case 3: $q_0/p_0 = 6$, $q_0/F = 226$,

Case 4: $q_0/p_0 = 8$, $q_0/F = 301.4$,

It can be observed from Fig. 5 that the displacements (*U*, *W*) vary linearly and monotonically in the transverse direction, respectively, and circumferential displacement (*V*) and all stress components display an obvious non-linear behavior. Fig. 5(d) implies that the radial stress at one point is independent from variation of loads ratio. As the Figs. 5 (e), (h) and (i) indicate, the stress component (σ_Θ, $\tau_{\Theta\xi}$, $\tau_{\eta\Theta}$) more affected by increasing the in-plane shear traction, especially in upper surface of the plate. It is logically expected, because the increase of tangential force causes extra moment relative to other tractions and consequently causes additional compression of the layers in the circumferential direction. It is observable from Fig. 5(f) that the distribution of stress (σ_ξ) along the thickness direction, especially in the top surfaces of the plate is independent from changes of in-plane shear traction. This behavior is obvious, because of the variation of transverse normal stress in the thickness direction mainly dependent to normal tractions and structure stiffness. As discussed earlier, the distribution of transverse shear stresses ($\tau_{\eta\xi}$, $\tau_{\Theta\xi}$) through the thickness of the plate shown in Figs. 5 (g) and (h) satisfy the boundary conditions, and the pick value of $\tau_{\eta\xi}$ enhances by the loads ratio increase. The distribution of shear stress ($\tau_{\eta\xi}$) versus thickness direction is parabolic and the pick value of this stress component increases by enhancing the loads ratio, as the Fig. 5(g) confirms.

In this subsection, the influence of coefficient of the elastic foundations on the static behavior of the plate is investigated. Results of Fig. 6 are depicted for a section located at (θ=30° and η=(a−b)/2) and k_{1o}, T_o, k_{uo}=*k*=1,5,10,15. It is evident that as the stiffness of elastic foundations increases, it will absorb much strain energy and subsequently, the resulting displacement and stresses become smaller, as Fig. 6 confirms. In this case the plate is subjected to compound and non-identical moments at the top and bottom layers, and radial movement is restricted at the outer edge, and the stress field approaches a hydrostatic state; so the normal stresses (σ_η, σ_Θ) become compressive/tensile for all points of the plate. For this reason, magnitudes of the transverse stresses become negligible. Furthermore, due to the elastic foundation

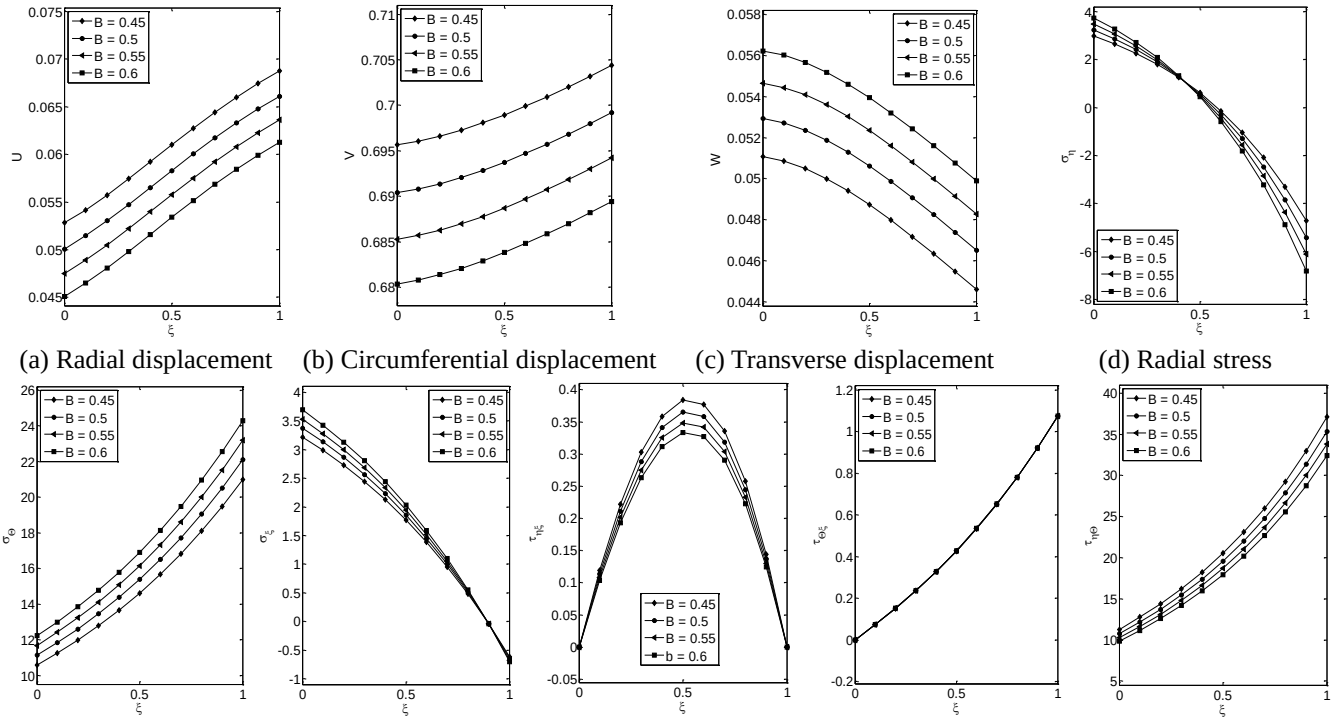

(a) Radial displacement (b) Circumferential displacement (c) Transverse displacement (d) Radial stress

(e) Tangential stress (f) Transverse normal stress (g) Transverse shear stress (h) Transverse shear stress (i) Tangential shear stress

Fig. 7 Effect of compressibility coefficient on the transverse distribution of mechanical entities of the simply supported circular plate at section η=(a−b)/2 and θ=π/6

reaction, the in-plane shear stress ($\tau_{\eta\Theta}$) of the lower surface of the plate is larger than the previous cases. The pick value of stress ($\tau_{\eta\xi}$) becomes less for higher values of foundation stiffnesses.

Example 4: In this example, a simply supported 2D-FGPM circular plate is considered and the effects of structure porosity and compressibility coefficient on the elastic field components are investigated. The other conditions are the same as those in example 2.

The effects of the compressibility coefficient (B) on the resulting displacement and stress components of the plate are demonstrated in Fig. 7, for a section at (η=(a−b)/2, θ=30°). It can be seen from Fig. 7(a, b) that the plate becomes more compliant and stiffer in transverse and radial directions as the compressibility coefficient of the plate increases; so that the radial and transverse stiffnesses of the plate increase and decrease, respectively. For this reason and due to in-plane traction the values of circumferential displacement (V) and stresses (σ_Θ, $\tau_{\eta\Theta}$) have increased. The stress (σ_η) transforms from tensile at lower surfaces of the plate to compressive at upper surfaces of the plate and its values decreases with increasing the compressibility coefficient at top layers. Furthermore, this stress component is independent from variations of compressibility at one point, as Fig. 7(d) implies.

The influence of the porosity of the structure of the plate is investigated considering four distinct porosity values (ϕ_p=0.01, 0.02, 0.04, 0.08). Due to presence of incompressible fluid content in the pores, increasing the porosity leads to a stiffer plate and consequently, to smaller displacement and stress components, as Fig. 8 confirms. Results of Fig. 8 are extracted for n_1=n_2=1, η=(a−b)/2 and θ=π/6. The Effect of the porosity on decreasing the displacement components becomes less for higher porosity values. Indeed, it can be observed that the influences of the porosity are opposite to those of the compressibility coefficient. Increasing the porosity has also decreased the σ_η and σ_Θ stress components of the top and bottom layers. However, location of the maximum transverse shear stress ($\tau_{\eta\xi}$) has almost remained unchanged. Furthermore, Figs. 7(h) and 8(h) reveal that the stress ($\tau_{\Theta\xi}$) is independent from compressibility and structure porosity variations.

4.2 Static analysis of the problem in the presence of foundation friction force

Example 5: In this example, a multidirectional FGPM circular plate with clamped edge, variable thickness, sinusoidal type tractions and elastic foundations as shown in Fig. 2 is considered. The effects of foundation graded exponents and foundation friction coefficient on the elastic field components are studied. The numerical data necessary to do the calculations is considered same as those in example 2.

The influence of the elastic foundation exponents on through-thickness distributions of mechanical quantities are reported in Fig.9. Results of this figure are plotted for the mid radius of the plate (η=(a−b)/2, θ=30°) and μ_1=μ_2=μ_3=μ=−0.8,−0.1,0.5,1, n_1=n_2=1, λ_1=λ_2=0.2. A quick glance at Fig. 9 reveals that the magnitudes of all displacement and stress components decrease by increasing the stiffness

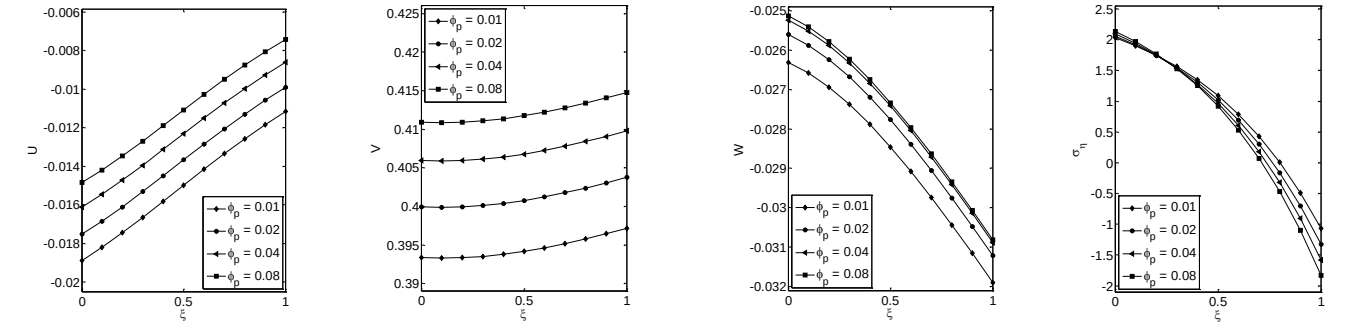

(a) Radial displacement (b) Circumferential displacement (c) Transverse displacement (d) Radial stress

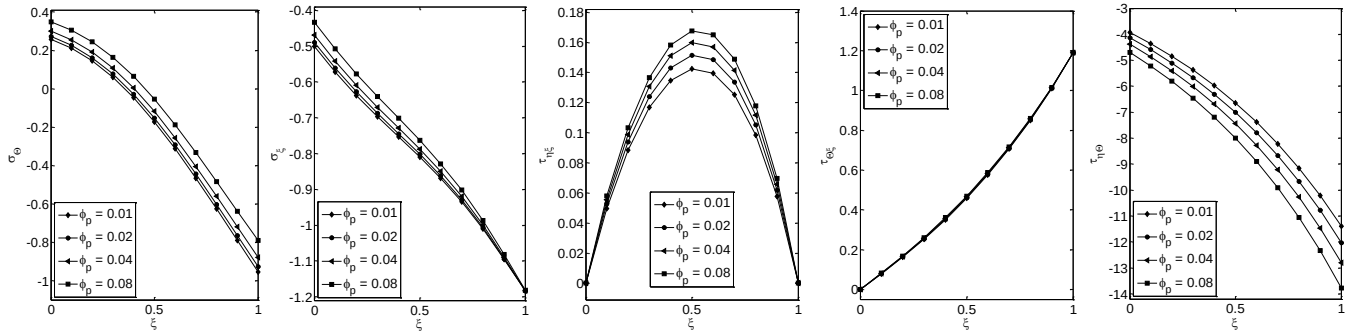

(e) Tangential stress (f) Transverse normal stress (g) Transverse shear stress (h) Transverse shear stress (i) Tangential shear stress

Fig. 8 Effect of the porosity on variation of mechanical entities across the plate thickness for a simply supported circular plate at η=(a−b)/2 and θ=π/6

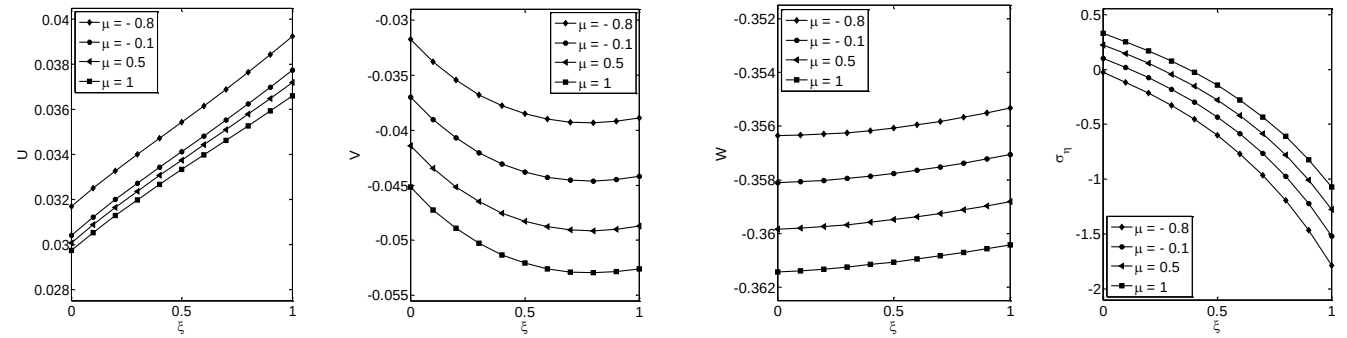

(a) Radial displacement (b) Circumferential displacement (c) Transverse displacement (d) Radial stress

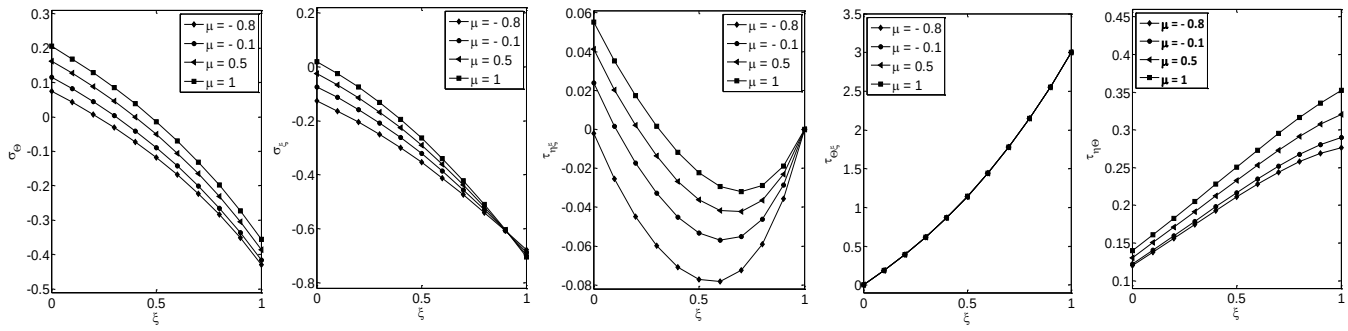

(e) Tangential stress (f) Transverse normal stress (g) Transverse shear stress (h) Transverse shear stress (i) Tangential shear stress

Fig. 9 Effect of the foundation graded indices on variation of mechanical entities across the plate thickness for a circular plate with clamped edge at η=(a−b)/2 and θ=π/3

exponent through regular trends. This behavior is logically expected, because: when the foundation graded exponents increase, the elastic foundation becomes stiffer and it absorbs much strain energy and consequently, the resulting displacements and stress components become smaller. Furthermore, due to the non-uniform foundation friction

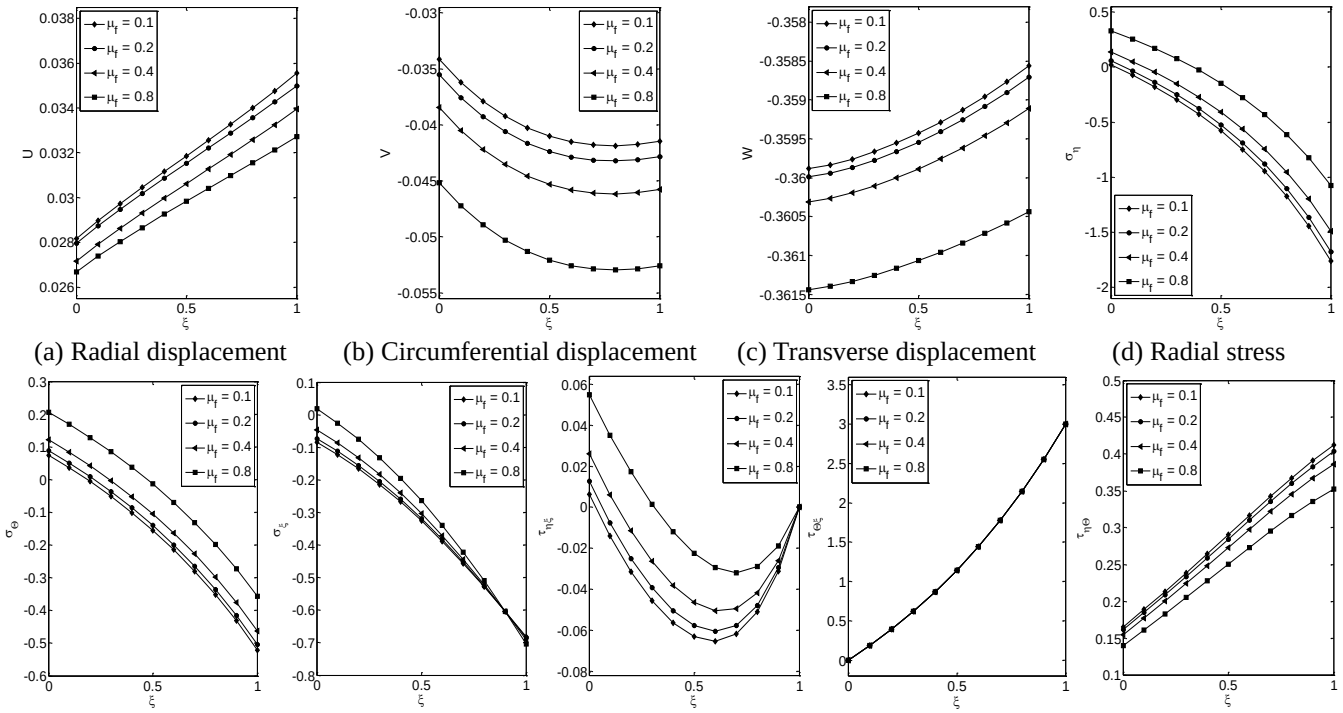

(a) Radial displacement (b) Circumferential displacement (c) Transverse displacement (d) Radial stress

(e) Tangential stress (f) Transverse normal stress (g) Transverse shear stress (h) Transverse shear stress (i) Tangential shear stress

Fig. 10 Effect of foundation friction coefficient variation on mechanical entities across the plate thickness for a circular plate with clamped edge at η=(a−b)/2 and θ=π/3

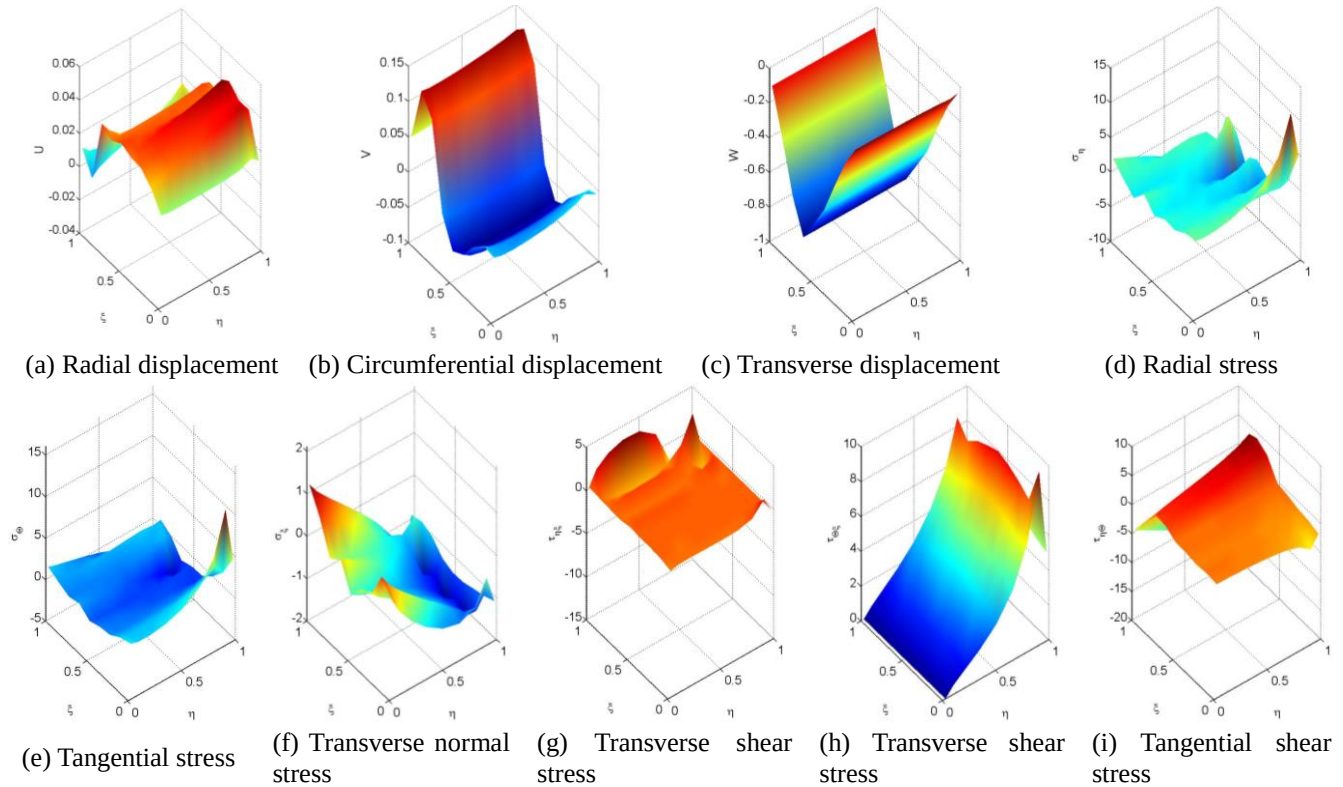

(a) Radial displacement (b) Circumferential displacement (c) Transverse displacement (d) Radial stress

(e) Tangential stress (f) Transverse normal stress (g) Transverse shear stress (h) Transverse shear stress (i) Tangential shear stress

Fig. 11 Three-dimensional representation of displacements and stress components distributions for a clamped circular plate at section θ=π/3

force which causes additional compression in the radial direction and rotation in the circumferential direction, the displacement (V) and stress ($\tau_{\eta\xi}$) exhibit more sensitivity relative to results discussed in Fig. 6.

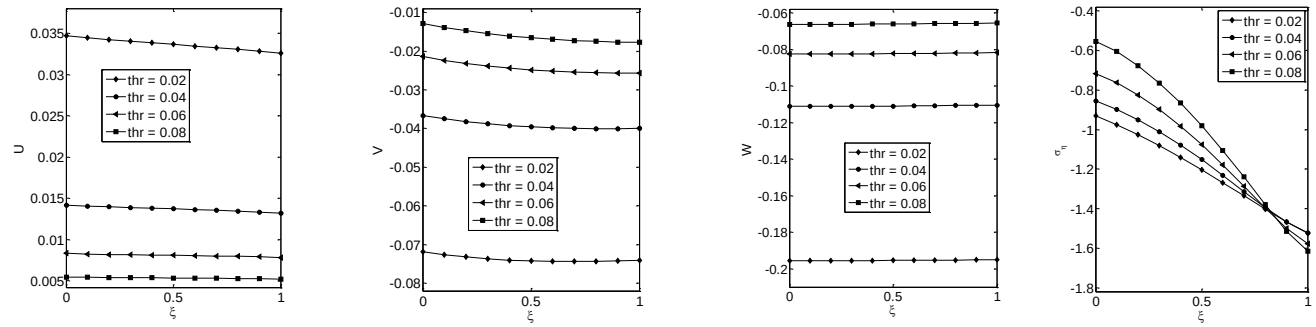

(a) Radial displacement (b) Circumferential displacement (c) Transverse displacement (d) Radial stress

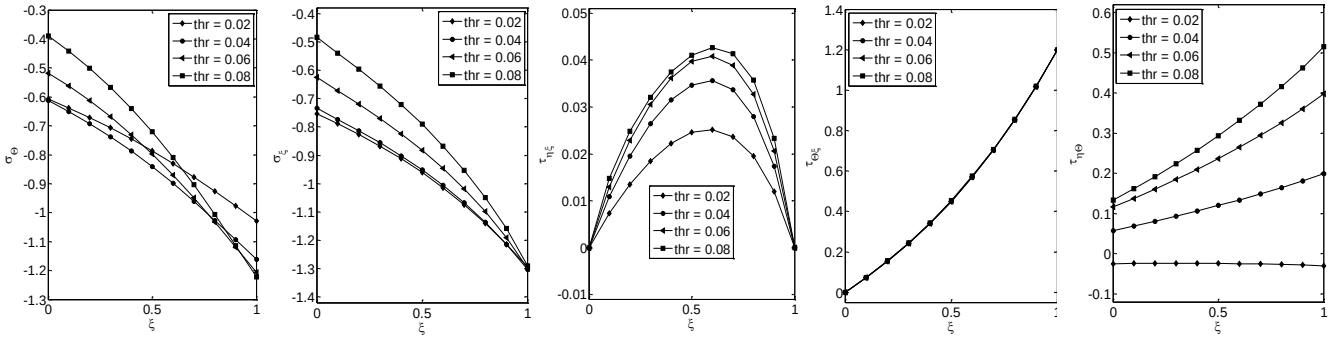

(e) Tangential stress (f) Transverse normal stress (g) Transverse shear stress (h) Transverse shear stress (i) Tangential shear stress

Fig. 12 Effect of thickness to radius ratio on mechanical entities across the plate thickness for a circular plate with clamped edge at η=(a−b)/2 and θ=π/3

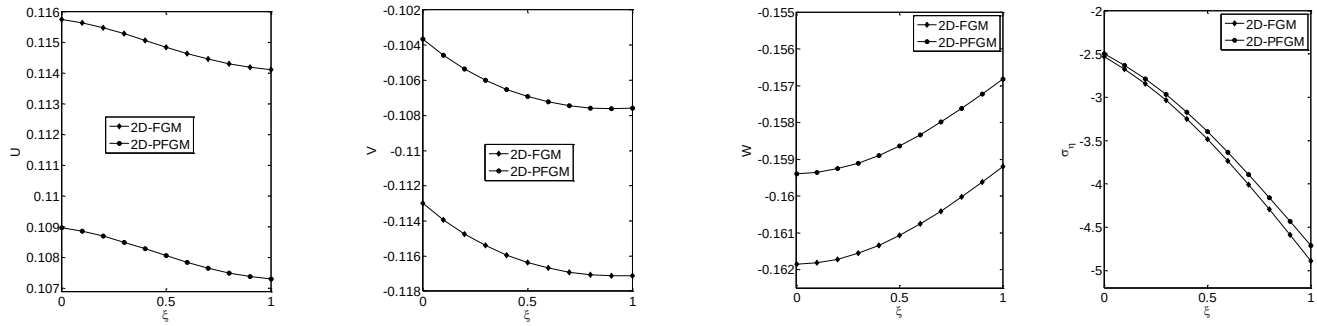

(a) Radial displacement (b) Circumferential displacement (c) Transverse displacement (d) Radial stress

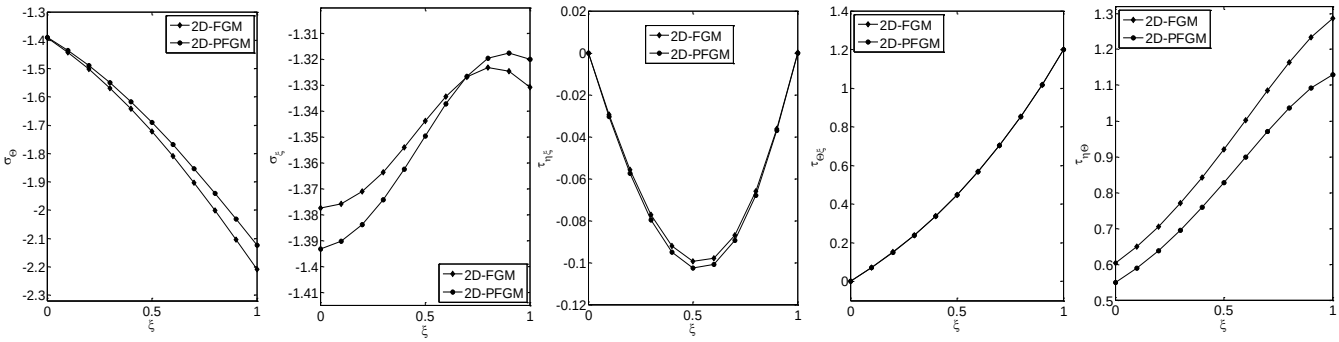

(e) Tangential stress (f) Transverse normal stress (g) Transverse shear stress (h) Transverse shear stress (i) Tangential shear stress

Fig. 13 Transverse distributions of displacements and stress components of the non-uniform circular plate with clamped edge and composed from heterogeneous and porous heterogeneous material at section η=(a−b)/2 and θ=π/4

The effect of the foundation friction coefficient is investigated in the results plotted in Fig. 10, for μ_1=μ_2=μ_3=1, λ_1=λ_2=0.2, μ_f=0.1,0.2,0.4,0.8 and a section located at (η=(a−b)/2, θ=60°). As Fig. 10 shows, magnitudes of all displacement and stress components decrease by increasing the friction coefficient through regular trends. Furthermore,

as Figs. 10(b), (c) and (g) reveal, rotations of the section, transverse deformation and stress ($\tau_{\eta\xi}$) are significantly affected by foundation friction coefficient changes.

Three dimensional representations of the simultaneous radial and transverse variations of the displacements and stress components of the clamped circular plate at section θ=60° are portrayed in Fig. 11. This figure reveals that all displacements and stress components display an obvious non-linear behavior. Furthermore, as figure implies, due to non-identical moments that exert in different planes and movement restriction of plate at clamped edge, the elastic field components exhibit rough and crispy distributions at adjacent of outer support.

In Fig. 12, the effect of the thickness to radius ratio on the static behavior of the porous heterogeneous plate is presented for $\mathrm{thr} = \hbar = 0.02, 0.04, 0.06, 0.08$ at location of radius midpoint and $\theta=\pi/3$. A quick glance at Fig. 12 reveals that the increase in the $\hbar$ causes decrease in U, V, W, σ_η, σ_ξ components, (U is tension). The pick value of $\tau_{\eta\xi}$ increases as the thickness to radius ratio increases. This feature is logically expected, because the distribution of transverse shear stress along the thickness direction for relative thick plates is quite parabolic while the distribution of this stress component for thin plates is parabolic with low pick value and tends to linear distribution. Furthermore, as Fig. 12(i) shows, the stress $\tau_{\eta\Theta}$ exhibits somewhat cubic distribution for high thickness to radius ratios.

In order to establish a comparative analysis, the dimensionless displacements and stress components are extracted to 2D-FG and 2D-FG porous circular plates at section $\theta=\pi/4$ and radius midpoint. The achieved results are illustrated in Fig. 13. As the figure shows, the magnitude of displacements and stresses (σ_η, σ_Θ, $\tau_{\eta\Theta}$) for porous FG plate are lower than the FG plate. It can be deduced the load carrying capacity of porous FG plate is high.

5. Conclusions

A three-dimensional elasticity solution is presented for static analysis of non-uniform functionally graded porous material circular plates resting on gradient hybrid elastic foundations including horizontal friction force, under non-uniform and asymmetric tractions. Results reveal that:

1) Exponents of the elasticity modulus significantly affect the location of the inflection section of the plate and consequently, distributions of the displacement and stress components are affected.

2) In stiffer foundations, the stress field approaches a hydrostatic state; so that magnitudes of the transverse stresses become negligible but the in-plane shear stress ($\tau_{\eta\Theta}$) of the plate becomes larger.

3) In the presence of in-plane traction, through thickness distribution of stress, ($\tau_{\Theta\xi}$) is independent from foundation coefficients, compressibility, porosity, foundation graded indices and foundation friction coefficient variations.

4) The porosity and compressibility coefficient exhibit opposite behavior on elastic field components.

5) Three dimensional theory of elasticity presents an accurate prediction of three axes Von-Misses stress, and as a result, it can accurately estimate the structure strength.

6) The effect of foundation friction force on displacements (U, V) and stress ($\tau_{\eta\xi}$) become more remarkable for greater friction coefficients.

7) Load carrying capacity of porous FG plate is higher than the FG plate.

8) The porosity has a very important role on the static behavior of the porous heterogeneous plates.

Acknowledgments

The authors would like to thank the reviewers for their valuable suggestions and comments, which are really helpful in revising the paper.

References

Abbasi, S., Farhatnia, F. and Jazi, SR. (2014), "A semi-analytical solution on static analysis of circular plate exposed to non-uniform axisymmetric transverse loading resting on Winkler elastic foundation", *Arch. Civil Mech. Eng.*, **14**(3), 476-488.

Akbas, S.D. (2017), "Post-buckling responses of functionally graded beams with porosities", *Steel Compos. Struct.*, **24**(5), 579-589.

Alibeigloo, A. and Simintan, V. (2011), "Elasticity solution of functionally graded circular and annular plates integrated with sensor and actuator layers using differential quadrature", *Compos. Struct.*, **93**, 2473-2486.

Alipour, M.M. and Shariyat, M. (2013), "Semi-analytical solution for buckling analysis of variable thickness two-directional functionally graded circular plates with non-uniform elastic foundations", *J. Eng. Mech.*, **139**(5), 664-676.

Asgari, M. (2015), "Material distribution optimization of 2D heterogeneous cylinder under thermo-mechanical loading", *Struct. Eng. Mech.*, **53**(4), 703-723.

Baccicchi, M., Elsenberger, M., Fantuzzi, N., Tornabene, F. and Viola, E. (2015), "Vibration analysis of variable thickness plates and shells by the generalized differential quadrature method", *Compos. Struct.*, **156**, 218-238.

Behravan Rad, A. (2012a), "Semi-analytical solution for functionally graded solid circular and annular plates resting on elastic foundations subjected to axisymmetric transverse loading", *Adv. Appl. Math. Mech.*, **4**(2), 205-222.

Behravan Rad, A. (2012b), "Static response of 2D functionally graded circular plate with gradient thickness and elastic foundations to compound loads", *Struct Eng. Mech.*, **44**(2), 139-161.

Behravan Rad, A. (2015), "Thermoelastic analysis of functionally graded circular plates resting on a gradient hybrid foundation", *Appl. Math. Comp.*, **256**, 276-298.

Behravan Rad, A. and Alibeigloo, A. (2013a), "Semi-analytical solution for the static analysis of 2D functionally graded circular and annular circular plates resting on elastic foundation", *Mech. Adv. Mater Struct.*, **20**(7), 515-528.

Behravan Rad, A. and Shariyat, M. (2013b), "A three-dimensional elasticity solution for two-directional FGM annular plates with non-uniform elastic foundations subjected to normal and shear tractions", *Acta Mech. Solida Sin*, **26**(6), 671-690.

Behravan Rad, A., Alibeigloo, A. and Malihi, S.S. (2010), "Static

analysis of functionally graded annular plate resting on elastic foundation subject to an axisymmetric transverse load, based on the three dimensional theory of elasticity", *J. Solid. Mech*., **2**(3), 290-304.

Benferhat, R., Daouadji, T.H., Mansour, M.S. and Hadji, L. (2016), "Effect of porosity on the bending and free vibration response of functionally graded plates resting on Winkler-Pasternak foundations", *Earthq. Struct.*, **10**(6), 1429-1449.

Chen, D., Yang, J. and Kitipornchai, S. (2015), "Elastic buckling and static bending of shear deformable functionally graded porous beam", *Compos. Struct.*, **133**, 54-61.

Chen, W.Q., Lu, C.F. and Bian, Z.G. (2004), "Free vibration analysis of generally laminated beams via state-space based differential quadrature", *Compos. Struct.*, **63**, 417-425.

Civalek, O. (2004a), "Application of differential quadrature (DQ) and harmonic differential quadrature (HDQ) for buckling analysis of thin isotropic plates and elastic columns", *Eng. Struct.*, **26**(2), 171-186.

Civalek, O. and Ulker, M. (2004), "Harmonic differential quadrature (HDQ) for axisymmetric bending analysis of thin isotropic circular plates", *Struct. Eng. Mech.*, **17**(1), 1-14.

Davoodi, K.I., Ghayour, M. and Mirdamadi, H.R. (2012), "Free vibration analysis of multi-directional functionally graded circular and annular plates", *Mech. Sci. Tech.*, **26**(11), 3399-3410.

Drawshi, M. and Betten, J. (1992), "Axially symmetric deformations and stability of a geometrically nonlinear circular plate subjected to multiparametrical static loading", *Arch. Appl. Mech.*, **62**, 455-462.

Fallah, F. and Nosier, A. (2012), "Non-linear behavior of functionally graded circular plates with various boundary supports under asymmetric thermo-mechanical loading", *Compos. Struct.*, **94**, 2834-2850.

Fallah, F., Vahidipoor, M.K. and Nosier, A. (2015), "Post-buckling behavior of functionally graded circular plates under asymmetric transverse and in-plane loadings", *Compos. Struct.*, **125**, 477-488.

Farzaneh Joubaneh, E., Mojahedin, A., Khorshidvand, A.R. and Jabbari, M. (2015), "Thermal buckling analysis of porous circular plate with piezoelectric sensor-actuator layers under uniform thermal load", *J. Sandw. Struct. Mater.*, **17**(1), 3-25.

Gupta, A. and Talha, M. (2015), "Recent development in modeling and analysis of functionally graded materials and structures", *Prog. Aero. Sci.*, **79**, 1-14.

Jabbari, M., Farzaneh Joubaneh, E. and Mojahedin, A. (2014a), "Thermal buckling analysis of a porous circular plate with piezoelectric actuators based on first order shear deformation theory", *Int. J. Mech. Sci.*, **83**, 57-64.

Jabbari, M., Farzaneh Joubaneh, E., Khorshidvand, A.R. and Eslami, M.R. (2013), "Buckling analysis of porous circular plate with piezoelectric actuator layers under uniform compression", *Int. J. Mech. Sci.*, **70**, 50-56.

Jabbari, M., Karampour, S. and Eslami, M.R. (2013), "Steady state thermal and mechanical stresses of a poro-piezo FGM hollow sphere", *Meccanica*, **48**, 699-719.

Jabbari, M., Mojahedin, A., Hashemitaheri, M. and Eslami, M.R. (2014b), "Thermal buckling analysis of functionally graded thin circular plate made of saturated porous materials", *J. Therm. Stress*, **37**(2), 202-220.

Jabbari, M., Mojahedin, A., Khorshidvand, A.R. and Eslami, M.R. (2014c), "Buckling analysis of a functionally graded thin circular plate made of saturated porous materials", *J. Eng. Mech.*, **140**(2), 287-295.

Jodaei, A. (2014), "3D elasticity solution for static analysis of functionally graded piezoelectric annular plates on elastic foundations using SSDQM", *Meccanica*, **49**(1), 215-237.

Khorshidvand, A.R., Farzaneh Joubaneh, E., Jabbari, M. and Eslami, M.R. (2014), "Buckling analysis of a porous circular plate with piezoelectric sensor-actuator layers under uniform radial compression", *Acta Mech.*, **225**, 179-193.

Kumar, Y. and Lal, R. (2013), "Prediction of frequencies of free axisymmetric vibration of two directional functionally graded annular plates on Winkler foundation", *Eur. J. Mech. A-Solid.*, **42**, 219-228.

Lal, R. and Ahlawat, N. (2015a), "Axisymmetric vibrations and buckling analysis of functionally graded circular plates via differential transform method", *Eur. J. Mech. A-Solid.*, **52**, 85-94.

Lal, R. and Ahlawat, N. (2015b), "Buckling and vibration of functionally graded non-uniform circular plates resting on Winkler foundation", *Latin Am. J. Solid. Struct.*, **12**, 2231-2258.

Li, X.Y., Ding, H.J. and Chen, W.Q. (2008), "Elasticity solutions for a transversely isotropic functionally graded circular plate subject to an axisymmetric transverse load qr^k", *Int. J. Solid. Struct.*, **45**(1), 191-210.

Malekzadeh, P., Golbahar Haghighi, M.R. and Atashi, M.M. (2011), "Free vibration analysis of elastically supported functionally graded annular plates subjected to thermal environment", *Meccanica*, **47**(2), 321-333.

Mojahedin, A., Jabbari, M., Khorshidvand, A.R. and Eslami, M.R. (2016), "Buckling analysis of a functionally graded plates made of saturated porous materials based on higher order shear deformation theory", *Thin Wall. Struct.*, **99**, 83-90.

Nie, G.J. and Zhong, Z. (2007), "Semi-analytical solution for three dimensional vibration of functionally graded circular plates", *Comput. Meth. Appl. Mech. Eng.*, **196**, 4901-4910.

Nie, G.J. and Zhong, Z. (2007a), "Axisymmetric bending of two-directional functionally graded circular and annular plates", *Acta Mech. Solida Sin.*, **20**(4), 289-295.

Saidi, A.R., Rasouli, A. and Sahraee, S. (2009), "Axisymmetric bending and buckling analysis of thick functionally graded circular plates using unconstrained third-order shear deformation plate theory", *Compos. Struct.*, **89**(1), 110-119.

Sburlati, R. and Bardella, L. (2011), "Three-dimensional elastic solutions for functionally graded circular plates", *Eur. J. Mech. A-Solid.*, **30**, 219-235.

Sepahi, O., Forouzan, M.R. and Malekzadeh, P. (2010), "Large deflection analysis of thermo-mechanical loaded annular FGM plates on nonlinear elastic foundation via DQM", *Compos. Struct.*, **92**(10), 2369-2378.

Shariyat, M. and Alipour, M.M. (2011), "Differential transform vibration and modal stress analyses of circular plates made of two-directional functionally graded materials resting on elastic foundations", *Arch. Appl. Mech.*, **81**(9), 1289-1306.

Sladek, J., Sladek, V., Stanak, P. and Hrcek, S. (2015), "Bending of a porous piezoelectric cylinder under a thermal load", *Eng. Anal. Bound. Elem.*, **51**, 136-145.

Swaminathan, K., Naveenkumar, D.T., Zenkour, A.M. and Carrera, E. (2015), "Stress, vibration and buckling analyses of FGM plates: a state-of-the-art review", *Compos. Struct.*, **120**, 10-31.

Tahouneh, V. and Yas, M.H. (2014), "Semi-analytical solution for three dimensional vibration analysis of thick multidirectional functionally graded annular sector plates under various boundary conditions", *J. Eng. Mech.*, **140**(1), 31-46.

Tornabene, F., Fantuzzi, N. and Baccicchi, M. (2016), "The local GDQ method for the natural frequencies of doubly-curved shells with variable thickness: A general formulation", *Compos. Part B: Eng.*, **92**, 265-289.

Wang, Y., Ding, H.J. and Xu, R.Q. (2016), "Three-dimensional analytical solutions for the axisymmetric bending of functionally graded annular plates", *Appl. Math. Model.*, **40**, 5393-5420.

Wang, Y., Xu, R.Q. and Ding, H.J. (2010), "Three-dimensional solution of axisymmetric bending of functionally graded

circular plates", *Compos. Struct.*, **92**, 1683-1693.
Wirowski, A., Michalak, B. and Gajdzicki, M. (2015), "Dynamic modeling of annular plates of functionally graded structure resting on elastic heterogeneous foundation with two modules", *J. Mech.*, **31**(5), 493-504.
Wu, C.P. and Liu, Y.C. (2016), "A review of semi-analytical numerical methods for laminated composites and multilayered functionally graded elastic/piezoelectric plates and shells", *Compos. Struct.*, **147**(1), 1-15.
Yang, B., Chen, W.Q. and Ding, H.J. (2014), "Approximate elasticity solution for functionally graded circular plates subjected to a concentrated force at the center", *Math. Mech. Solid.*, **19**(3), 277-288.
Yas, M.H. and Moloudi, N. (2015), "Three-dimensional free vibration analysis of multi-directional functionally graded piezoelectric annular plates on elastic foundations via state space based differential quadrature method", *Appl Math Mech.*, **36**(4), 439-464.
Yas, M.H. and Tahouneh, V. (2012), "3D free vibration analysis of thick functionally graded annular plates on Pasternak elastic foundation via differential quadrature method (DQM)", *Acta Mech*., **223**(1), 43-62.

CC

Appendix

1. Elements of state matrix at discretized points

$$D_i=\begin{bmatrix} [0]_{N\times N} & [0]_{N\times N} & [0]_{N\times N} \\ [0]_{N\times N} & [0]_{N\times N} & [0]_{N\times N} \\ [0]_{N\times N} & [0]_{N\times N} & [0]_{N\times N} \\ [d_{ij}^{41}]_{N\times N} & [d_{ij}^{42}]_{N\times N} & [d_{ij}^{43}]_{N\times N} \\ [d_{ij}^{51}]_{N\times N} & [d_{ij}^{52}]_{N\times N} & [d_{ij}^{53}]_{N\times N} \\ [d_{ij}^{61}]_{N\times N} & [d_{ij}^{62}]_{N\times N} & [d_{ij}^{63}]_{N\times N} \end{bmatrix}$$

$$\begin{bmatrix} [\delta_{ij}]_{N\times N} & [0]_{N\times N} & [0]_{N\times N} \\ [0]_{N\times N} & [\delta_{ij}]_{N\times N} & [0]_{N\times N} \\ [0]_{N\times N} & [0]_{N\times N} & [\delta_{ij}]_{N\times N} \\ [d_{ij}^{44}]_{N\times N} & [d_{ij}^{45}]_{N\times N} & [d_{ij}^{46}]_{N\times N} \\ [d_{ij}^{54}]_{N\times N} & [d_{ij}^{55}]_{N\times N} & [d_{ij}^{56}]_{N\times N} \\ [d_{ij}^{64}]_{N\times N} & [d_{ij}^{65}]_{N\times N} & [d_{ij}^{66}]_{N\times N} \end{bmatrix}_{6N\times 6N}$$

where $\delta_{ij}=0\,(i\neq j)$; $\delta_{ii}=1$

$$d_{ii}^{41}=-\left(\frac{\bar{C}_{11}^{0}}{\bar{C}_{55}^{0}}\right)(\hbar)^2\chi_{1i}^2\left\{A_{ii}^{(2)}+\left(\frac{1}{\eta_i}+\frac{n_2}{1-b/a}+2\chi_{2i}\right)\cdot A_{ii}^{(1)}+\left[\left(\frac{1}{\eta_i}+\frac{n_2}{1-b/a}\right)\chi_{2i}+\chi_{3i}-\frac{1}{\eta_i^2}\right]\right\}$$

$$-\left(\frac{\bar{C}_{12}^{0}}{\bar{C}_{55}^{0}}\right)(\hbar)^2\chi_{1i}^2\frac{n_2}{\eta_i(1-b/a)}+\left(\frac{\bar{C}_{66}^{0}}{\bar{C}_{55}^{0}}\right)(\hbar)^2\chi_{1i}^2\frac{1}{\eta_i^2}\quad (i=j)$$

$$d_{ij}^{41}=-\left(\frac{\bar{C}_{11}^{0}}{\bar{C}_{55}^{0}}\right)(\hbar)^2\chi_{1i}^2\left[\sum_{j=1}^{N}A_{ij}^{(2)}+\left(\frac{1}{\eta_i}+\frac{n_2}{1-b/a}+2\chi_{2i}\right)\sum_{j=1}^{N}A_{ii}^{(1)}\right]\quad (i\neq j)$$

$$d_{ii}^{42}=-\left(\frac{\bar{C}_{11}^{0}}{\bar{C}_{55}^{0}}\right)(\hbar)^2\chi_{1i}^2\frac{1}{\eta_i}\left[A_{ii}^{(1)}+\left(\frac{n_2}{1-b/a}+\chi_{2i}\right)\right]+\left(\frac{\bar{C}_{22}^{0}}{\bar{C}_{55}^{0}}\right)(\hbar)^2\chi_{1i}^2\frac{1}{\eta_i^2}$$

$$-\left(\frac{\bar{C}_{66}^{0}}{\bar{C}_{55}^{0}}\right)(\hbar)^2\chi_{1i}^2\left[\frac{1}{\eta_i}A_{ii}^{(1)}+\left(\frac{\chi_{2i}}{\eta_i}-\frac{1}{\eta_i^2}\right)\right]\quad (i=j)$$

$$d_{ij}^{42}=-\left(\frac{\bar{C}_{11}^{0}+\bar{C}_{66}^{0}}{\bar{C}_{55}^{0}}\right)(\hbar)^2\chi_{1i}^2\frac{1}{\eta_i}\sum_{j=1}^{N}A_{ij}^{(1)}\quad (i\neq j)$$

$$d_{ii}^{43}=-n_1\hbar\chi_{1i}\left(A_{ii}^{(1)}+\chi_{2i}\right)\quad (i=j)\ ,$$

$$d_{ij}^{43}=-n_1\hbar\chi_{1i}\sum_{j=1}^{N}A_{ij}^{(1)}\quad (i\neq j)$$

$$d_{ii}^{44}=-n_1\quad (i=j),\quad d_{ij}^{44}=0\quad (i\neq j)$$

$$d_{ii}^{46}=-\left(\frac{\bar{C}_{13}^{0}}{\bar{C}_{55}^{0}}\right)\hbar\chi_{1i}\left[A_{ii}^{(1)}+\left(\chi_{2i}+\frac{n_2}{1-b/a}+\frac{1}{\eta_i}\right)\right]+$$

$$\left(\frac{\bar{C}_{23}^{0}}{\bar{C}_{55}^{0}}\right)\hbar\chi_{1i}\frac{1}{\eta_i}-\hbar\chi_{1i}\left(A_{ii}^{(1)}+\chi_{2i}\right)\quad (i=j)$$

$$d_{ij}^{46}=-\left(\frac{\bar{C}_{13}^{0}}{\bar{C}_{55}^{0}}+1\right)\hbar\chi_{1i}\sum_{j=1}^{N}A_{ij}^{(1)}\quad(i\neq j)$$

$$d_{ii}^{51}=\left(\frac{\bar{C}_{12}^{0}}{\bar{C}_{44}^{0}}\right)\hbar^{2}\chi_{1i}^{2}\frac{1}{\eta_i}\left(A_{ii}^{(1)}+\chi_{2i}\right)+\left(\frac{\bar{C}_{22}^{0}}{\bar{C}_{44}^{0}}\right)\hbar^{2}\chi_{1i}^{2}\frac{1}{\eta_i^{2}}$$
$$+\left(\frac{\bar{C}_{66}^{0}}{\bar{C}_{44}^{0}}\right)\hbar^{2}\chi_{1i}^{2}\left\{\frac{1}{\eta_i}A_{ii}^{(1)}+\left[\frac{1}{\eta_i}\left(\chi_{2i}+\frac{n_2}{1-b/a}\right)+\frac{1}{\eta_i^{2}}\right]\right\}\quad(i=j)$$

$$d_{ij}^{51}=\left(\frac{\bar{C}_{12}^{0}+\bar{C}_{66}^{0}}{\bar{C}_{55}^{0}}\right)\hbar^{2}\chi_{1i}^{2}\frac{1}{\eta_i}\sum_{j=1}^{N}A_{ij}^{(1)}\quad(i\neq j)$$

$$d_{ii}^{52}=-\left(\frac{\bar{C}_{66}^{0}}{\bar{C}_{44}^{0}}\right)\hbar^{2}\chi_{1i}^{2}\left\{A_{ii}^{(2)}+\left(2\chi_{2i}+\frac{1}{\eta_i}+\frac{n_2}{1-b/a}\right)A_{ii}^{(1)}\right.$$
$$\left.+\left[\chi_{2i}+\chi_{3i}+\left(\chi_{2i}-\frac{1}{\eta_i}\right)\frac{n_2}{1-b/a}-\frac{1}{\eta_i^{2}}\right]\right\}$$
$$+\left(\frac{\bar{C}_{22}^{0}}{\bar{C}_{44}^{0}}\right)\hbar^{2}\chi_{1i}^{2}\frac{1}{\eta_i^{2}}\quad(i=j)$$

$$d_{ij}^{52}=-\left(\frac{\bar{C}_{66}^{0}}{\bar{C}_{44}^{0}}\right)\hbar^{2}\chi_{1i}^{2}\left[\sum_{j=1}^{N}A_{ij}^{(2)}+\left(2\chi_{2i}+\frac{1}{\eta_i}+\frac{n_2}{1-b/a}\right)\sum_{j=1}^{N}A_{ij}^{(1)}\right]\quad(i\neq j)$$

$$d_{ii}^{53}=-n_1\hbar\chi_{1i}\frac{1}{\eta_i}\quad(i=j)\quad,\quad d_{ij}^{53}=0\quad(i\neq j)$$

$$d_{ii}^{55}=-n_1\quad(i=j)\quad,\quad d_{ij}^{55}=0\quad(i\neq j),$$

$$d_{ii}^{56}=-\frac{1}{\eta_i}\left(\frac{\bar{C}_{23}^{0}}{\bar{C}_{44}^{0}}\right)\quad(i=j)\quad,\quad d_{ij}^{56}=0\quad(i\neq j)$$

$$d_{ii}^{61}=-n_1\left(\frac{\bar{C}_{13}^{0}}{\bar{C}_{33}^{0}}\right)\hbar\chi_{1i}\left[A_{ii}+\left(\chi_{2i}+\frac{1}{\eta_i}\right)\right]\quad(i=j),$$

$$d_{ij}^{61}=-n_1\left(\frac{\bar{C}_{13}^{0}}{\bar{C}_{33}^{0}}\right)\hbar\chi_{1i}\sum_{j=1}^{N}A_{ij}\quad(i\neq j)$$

$$d_{ii}^{62}=-n_1\left(\frac{\bar{C}_{23}^{0}}{\bar{C}_{33}^{0}}\right)\hbar\chi_{1i}\frac{1}{\eta_i}\quad(i=j),\quad d_{ij}^{62}=0\quad(i\neq j)$$

$$d_{ii}^{63}=-\left(\frac{\bar{C}_{44}^{0}}{\bar{C}_{33}^{0}}\right)\hbar^{2}\chi_{1i}^{2}\left\{A_{ii}^{(2)}+\left(\frac{1}{\eta_i}+2\chi_{2i}+\frac{n_2}{1-b/a}\right)A_{ii}^{(1)}\right.$$
$$\left.+\left[\chi_{3i}+\chi_{2i}\left(\frac{1}{\eta_i}+\frac{n_2}{1-b/a}\right)-\frac{1}{\eta_i^{2}}\right]\right\}\quad(i=j)$$

$$d_{ij}^{63}=-\left(\frac{\bar{C}_{44}^{0}}{\bar{C}_{33}^{0}}\right)\hbar^{2}\chi_{1i}^{2}\left[\sum_{j=1}^{N}A_{ij}^{(2)}+\left(\frac{1}{\eta_i}+2\chi_{2i}+\frac{n_2}{1-b/a}\right)\sum_{j=1}^{N}A_{ij}^{(1)}\right]\quad(i\neq j)$$

$$d_{ii}^{64}=-\left(\frac{\bar{C}_{13}^{0}}{\bar{C}_{33}^{0}}\right)\hbar\chi_{1i}\left[A_{ii}+\left(\chi_{2i}+\frac{1}{\eta_i}\right)\right]-$$
$$\left(\frac{\bar{C}_{55}^{0}}{\bar{C}_{33}^{0}}\right)\hbar\chi_{1i}\left[A_{ii}+\left(\chi_{2i}+\frac{n_2}{1-b/a}+\frac{1}{\eta_i}\right)\right]\quad(i=j)$$

$$d_{ij}^{64}=-\left(\frac{\bar{C}_{13}^{0}+\bar{C}_{55}^{0}}{\bar{C}_{33}^{0}}\right)\hbar\chi_{1i}\sum_{j=1}^{N}A_{ij}^{(1)}\quad(i\neq j)$$

$$d_{ii}^{65}=-\left(\frac{\bar{C}_{23}^{0}}{\bar{C}_{44}^{0}}\right)\frac{\hbar\chi_{1i}}{\eta_i}\quad(i=j),\ d_{ij}^{65}=0\quad(i\neq j),$$

$$d_{ii}^{66}=-n_1\quad(i=j),\ d_{ij}^{66}=0\quad(i\neq j)$$
$$i=1,2,3,\ \ldots,N\qquad\text{(A1)}$$

2. Elements of concentrated force matrix

$$B_i=\begin{bmatrix}[0]_{N\times N}&[0]_{N\times N}&[0]_{N\times N}&[0]_{N\times N}&[0]_{N\times N}&[0]_{N\times N}\\ [0]_{N\times N}&[0]_{N\times N}&[0]_{N\times N}&[0]_{N\times N}&[0]_{N\times N}&[0]_{N\times N}\\ [0]_{N\times N}&[0]_{N\times N}&[0]_{N\times N}&[0]_{N\times N}&[0]_{N\times N}&[0]_{N\times N}\\ [0]_{N\times N}&[0]_{N\times N}&[0]_{N\times N}&\left[b_{ij}^{44}\right]_{N\times N}&[0]_{N\times N}&[0]_{N\times N}\\ [0]_{N\times N}&[0]_{N\times N}&[0]_{N\times N}&\left[b_{ij}^{54}\right]_{N\times N}&[0]_{N\times N}&[0]_{N\times N}\\ [0]_{N\times N}&[0]_{N\times N}&[0]_{N\times N}&\left[b_{ij}^{64}\right]_{N\times N}&[0]_{N\times N}&[0]_{N\times N}\end{bmatrix}_{6N\times 6N}$$

$$b_{i1}^{44}=\Gamma_i d_{i1}^{44}\quad(j=1),\ b_{ij}^{44}=0\quad(j\neq 1)$$
$$b_{i1}^{54}=\Gamma_i d_{i1}^{54}\quad(j=1),\ b_{ij}^{54}=0\quad(j\neq 1)$$
$$b_{i1}^{64}=\Gamma_i d_{i1}^{64}\quad(j=1),\ b_{ij}^{64}=0\quad(j\neq 1)$$
$$i,j=1,2,3,\ldots,N\qquad\text{(A2)}$$